Analytical and Numerical Study of Fire-Damaged Circular Concrete Columns Repaired Using Composite Confinement Techniques

Iqrar Hussain[3]*, M. Yaqub[1], Mina Mortazavi[2], M. Adeel[3], M. Uzair[3]

1. Professor Dr, Department of Civil Engineering, University of Engineering & Technology, Taxila, 47080, Pakistan

2. Lecturer Dr, School of Civil and Environmental Engineering, University of Technology Sydney, NSW 2007, Australia

3. Research Scholars, Department of Civil Engineering, University of Engineering & Technology, Taxila, 47080, Pakistan

*Corresponding author, iqrar.turi73@gmail.com

Abstract

This paper presents numerical and statistical modeling of 21 undamaged, fire-damaged and repaired fire-damaged reinforced circular concrete columns. After casting the columns were exposed to three temperatures of 300°C, 500°C and 900°C and tested for axial residual capacity. Fire-damaged columns were repaired using various confinement techniques. Numerical models for undamaged, fire-damaged and repaired fire-damaged columns were developed using the concrete plasticity damage model available in finite element analysis software Abaqus. Analytical equations were developed using linear, multiple and quadratic regression modeling. The analytical and numerical models were found to be in good agreement with the experimental results and the models could reasonably predict the experimental load–deformation response of undamaged, fire-damaged and repaired fire-damaged circular columns.

Keywords: Numerical model, analytical model, axial load–deformation response, fire-damaged columns, composite confinement repair techniques

1. Introduction

Damage to buildings from fire incidents has been increasing globally. Fire can affect the structural integrity of buildings built with concrete as it is well-known that the material properties of concrete structures are affected during and after fire incidents [1]. For instance, a

42% reduction in strength of reinforced concrete columns is noted after being subjected to a temperature of 500°C [2]. As well as a reduction in compressive and flexural strengths, heat has a significant effect on mechanical properties like modulus of elasticity and volume stability [3]. Experiences have shown that after fire events, the reinstatement of fire-damaged buildings is preferable both technically and cost-effectively to rebuilding or demolition. The gunite repair is the most conventional method used to reinstate fire-damaged reinforced concrete structures. However, due to the disruptive and time consuming process, construction engineers are seeking new advanced repair techniques to ensure that following a fire buildings are recommissioned as inexpensively, effectively and rapidly as possible. Previous studies have shown that the use of fiber-reinforced polymer (FRP) jacketing is a rapid and effective solution to repair, strengthen and retrofit existing damaged structures [4]. The load–deformation capacity of reinforced concrete columns is the most important mechanical property and it has a major contribution to the stability of a concrete structure during extreme loading. Previous studies have clearly shown that the axial load–deformation capacity of columns decreases as the temperature increases. The assessment of the residual capacity of repaired columns after heat damage is very complicated due to non-uniform temperature distribution during fire exposure within the cross-section of columns. Practicing engineers need a simplified economical procedure to assess the stability of fire-damaged reinforced concrete structures after reinstatement to ensure that residual capacity meets functional requirements. To observe the failure modes and the actual behavior of reduced scale structures, laboratory tests on structural elements are essential. However, this practical testing is expensive, time consuming and often limits the pace of research progress. Moreover, because of the limitations of equipment, existing structures cannot be tested at ultimate failure and the scale effect cannot be observed at large scale experimentally. Thus numerical and analytical studies are required to predict the behavior of fire-damaged and repaired fire-damaged structures to reduce the cost in terms of time and experimental expenses.

The importance of structural performance after fire makes this study vital to predict the response of fire-damaged structures repaired with various composite confinement techniques. With the development of computer technology and increasing demand for advanced structural analysis, it is a simpler, more convenient, easier and time-saving approach. A number of analytical equations and numerical models have been developed in the past to predict the load-carrying

capacity and the corresponding deformations of FRP confined plain concrete cylinders or reinforced concrete columns without any fire damage. To the best of the authors' knowledge, currently, limited finite element modeling research is available to assess the behavior of FRP confined reinforced concrete circular columns after fire damage [5–7].

Many researchers have concentrated on using multivariable regression models to improve the accuracy of predictions and to develop relationships for the axial capacity of high performance concrete [8, 9]. Chopra and Kumar used regression to predict the compressive strength of concrete with and without fly ash [10]. In combination with artificial neural networks, the multiple regression model has also been used to predict the strength of mineral concrete [11]. However, linear relationships have uncertainties and that term must be considered as an error term in the regression model. Uncertainties in using empirically-derived models for design purposes have increased interest in the use of finite element modeling to gain a better understanding of the behavior of confined concrete. Many attempts have been made to model circular columns subjected to different conditions through the use of computational techniques such as finite element analysis [12–14]. Finite element numerical simulation has been used by many researchers to predict the behavior of carbon fiber reinforced polymer-confined concrete cylinders or columns with different wrapping materials and bonding dimensions [15–17]. Bikhiet et al. created a nonlinear finite element model to check the behavior of post-heated reinforced concrete columns and the simulation showed the high effect of temperature on stress and its distribution [12, 18]. Abaqus software is a preferred tool used by researchers in finite element analysis. This tool is actually an implicit analysis program with the constitutive model [19–24].

In modern structural engineering, interest in the development of analytical equations based on regression of test data and finite element modeling has increased to gain a better understanding of the axial load–deformation behavior of fire-damaged concrete circular columns repaired using different composite FRP confinement techniques. The behavior of FRP confined concrete cylinders or reinforced concrete columns with different wrapping materials has been accurately predicted by many researchers using finite element modeling. However, to the best of the authors' knowledge, all the published research work is limited to unheated concrete. In the literature limited studies have been reported on the finite element modeling of the repair of post-

heated reinforced concrete circular columns using CFRP confinement repair techniques. Therefore, there is a gap in experimental, regression and numerical studies on the repair of reinforced concrete circular columns after fire using different composite confinement techniques.

In this paper, analytical and numerical models are proposed to predict the load–deformation response of undamaged, fire-damaged and repaired circular columns using different composite confinement techniques. The capacity of the numerical models and analytical equations to predict the axial load–deformation response of undamaged, fire-damaged and repaired fire-damaged reinforced concrete columns was validated with experimental studies. The experimental results in terms of axial load–deformation response are examined and compared with the finite element and regression model results. This paper provides an innovative analytical and finite element solution to assess the load–deformation response of undamaged, fire-damaged and fire-damaged reinforced concrete circular columns after reinstatement using different composite confinement repair techniques.

2. Experimental tests

The experimental study presented in this paper is part of a comprehensive research project to use innovative composite confinement repair techniques for fire-damaged concrete. The present experimental study consists of undamaged, fire-damaged and repaired fire-damaged medium-scale reinforced concrete circular columns tested at room temperature under uniaxial compression up to the failure. The columns were initially damaged by exposure to three different peak temperatures of 300ºC, 500ºC and 900ºC. The fire-damaged columns were then repaired using exclusively carbon fiber reinforced polymer jackets or using epoxy resin mortar injected steel wire mesh jointly confined with carbon fiber reinforced polymer jackets.

2.1 Material properties

The concrete columns were cast using Fauji (Ordinary Portland) cement manufactured in Pakistan, Lawrancepur sand passing No.8 Sieve, and Margala crush. All the aggregates were used as per ASTM C 33-08 grading 67 criteria. The maximum size of the aggregates was 19 mm. Polypropylene fiber was also used in mixing the concrete to cast the specimens to avoid explosive spalling. Chemdur 300 as an epoxy adhesive along with dry carbon fiber reinforced

4

polymer wrap was used. Welded steel wire mesh was used to confine the concrete members to enhance load carrying capacity and stiffness. All the columns were cast in accordance with ASTM C-31 specifications and under local environmental conditions. Tables 1–5 summarize the properties of polypropylene (Sika Fiber 12) dry carbon fiber reinforced polymer (CFRP Wrap CFW-600), epoxy adhesive for carbon-fiber wrapping (Chemdur 300), epoxy adhesive and repair mortar (Sikadur 31 CF Slow) and welded steel wire mesh provided by the manufacturers.

2.2 Casting and heating

A total of 21 reinforced concrete circular columns (specimens) (H = 1200 mm and D = 200 mm) were cast, categorized into four groups for heating and repairing with different advanced and smart repair and strengthening materials (see Table 6). For all columns, eight 6 mm diameter deformed bars were used as ties and link reinforcement with spacing 150 mm center to center. All of the specimens were properly cured. Prior to the application of load, the reinforced concrete columns were heated in an industrial furnace Heavy Mechanical Complex at Taxila in Pakistan, at three different temperatures: 300°C, 500°C and 900°C (refer to Figure 1). This study is focused on peak temperature in the furnace because of the reason that the realistic heating of concrete is being reflected or simulated by standard fire. External Peak Temperature and duration of fire are the factors effecting the severity of fire in real fire incident. During the real fire incident, the outer layer of concrete is more vulnerable as compared to the inner core because of the higher temperature on the outer layer. The maximum temperature and time recorded in this study are presented by the time–temperature curve shown in Figure 2. Six specimens were post-heated not repaired, six post-heated specimens were CFRP wrapped, and six specimens were air-cured confined with steel wire mesh following by CFRP wrapping. The repaired samples were tested and the axial load–axial deformation curve was noted.

3. Finite element modeling

A nonlinear finite element analysis capable of predicting the axial load–deformation behavior of undamaged, fire-damaged and fire-damaged reinforced concrete circular columns repaired with different composite confinement techniques was carried out using commercial software Abaqus Standard 6.12. Abaqus Standard efficiently, accurately and reliably provides a wide range of linear and nonlinear engineering simulations.

3.1 Material modeling

The exact material behavior modeling in finite element analysis plays a very important role in capturing the predictions of numerical results closer to experimental values. The major aspects of modeling columns are the homogeneous solid concrete section, transverse and longitudinal reinforcements. The following approach was adopted to model the behavior of concrete and reinforcement in the circular columns.

3.1.1 Concrete

A concrete damage plasticity model available in Abaqus Standard was used to simulate the behavior of concrete in circular columns. The concrete damage plasticity model has the capability to model plain concrete, reinforced concrete, and other quasi-brittle materials in all types of structures including beams, trusses, shells and solids [14, 25, 26]. This model consists of two main damage failure mechanisms: tensile cracking and compressive crushing of concrete. The model assumes that the uniaxial tensile and compressive response of concrete is characterized by damaged plasticity [27–29].

Compressive crushing and tensile cracking are actually two mechanisms of concrete defined by concrete damage plasticity models. In the present study, the behavior of concrete for controlled samples was defined by the concrete damage plasticity model given by Liu et al. [19, 30]. The concrete damage plasticity model in Abaqus consists of plastic behavior, compressive behavior and tensile behavior of concrete. The linear proportional limit of concrete was assumed to be equal to 0.4 times the cylindrical compressive strength of concrete [31]. The post-failure behavior is defined in terms of stress cracking displacement relationships available in Abaqus Standard. An experimental study shows that concrete has different behavior in compression and tension. The tensile strength of concrete is typically 8–15% of the compressive strength [32, 33]. The stress–strain curve of concrete is approximately linearly elastic in tension up to the maximum tensile strength. After reaching the elastic limit, the concrete cracks and the strength decreases gradually to zero [34]. The Poisson ratio of concrete under uniaxial compressive stress is approximately 0.2. The 28-day maximum compressive strength occurs between a strain of approximately 0.002 to 0.003. The maximum usable strains can be taken as 0.003 for the

6

strength of concrete [35, 36]. The properties of concrete used in the model are shown in Table 7. The elastic modulus and Poisson's ratio represent the elastic properties of concrete. The unconfined behavior of concrete was used to model the compressive behavior of both unheated and post-heated concrete control specimens. The equations given by Eurocode BS EN1992-1-1 and BS EN1994-1-2 were used to model the nonlinear compressive stress–strain behavior. The curve given by BS EN1992-1-1 is for unconfined unheated concrete while the curve given by BS EN1994-1-2 is for unconfined post-heated concrete. The Abaqus program requires the uniaxial stress–strain relationship for concrete in compression. To predict the nonlinear behavior of unheated unconfined concrete control specimens, the compressive stress–strain part of the curve was obtained using the equations based on BS EN 1992-1-1 [37]. Figure 3 and Figure 4 shows the compressive uniaxial stress–strain relationship of concrete used in the model. The modulus of elasticity of concrete was determined from the slope of the stress–strain relationship. The compressive stress–strain relationship used in this study, given by BS EN 1992-1-1, is for unheated concrete. The shape of the stress–strain curves of concrete does not change after heating. However, the peak in the curve is reduced due to induced degradation and occurs at a higher strain [38, 39]. Moreover, the slope of the descending portion of the stress–strain curves is reduced with increasing temperature [38]. The compressive strength of concrete will not recover to its initial value when it is heated to the maximum temperature of t_{max}, and allowed to cool down at ambient temperature [40]. BS EN1994-1-2 considers the same peak strain for concrete during heating and cooling. Therefore, in the descending branch of the concrete heating curve, as shown in Figure 4, the value of the slope of the descending branch of the stress–strain relationship may be maintained as equal to the corresponding values for t_{max}.

To predict the unconfined nonlinear behavior of fire-damaged reinforced concrete control specimens, the compressive stress–strain data calculated based on BS EN1994-1-2 [40] was adopted for fire-damaged concrete in this study. Mander et al. [41] proposed the first confinement model for the nonlinear compressive stress–strain behavior of concrete. ACI 440 2R-08 provided equations based on a model developed by Lam and Teng [42] which can be used to predict the compressive stress–strain behavior of FRP confined circular cylinders. The Lam and Tang model is also based on the nonlinear confined compressive stress–strain behavior of unheated concrete. Since the behavior of concrete softens with increasing temperature, the peak

in the curve is reduced due to induced degradation and occurs at a higher strain. To model the FRP confined nonlinear compressive stress–strain behavior of fire-damaged concrete, after exposure to three peak temperatures of 300°C, 500°C and 900°C, the concrete cylinders were repaired using two different composite confinement techniques and tested under axial compression. The confined stress–strain curves of post-heated concrete was used for FRP confined post-heated concrete in this study. The tensile part is assumed to be linear up to the ultimate tensile strength.

$$f_t' = 0.33\sqrt{f_c'} \qquad (MPa)$$

After this point, the concrete cracks and is expressed in terms of the stress cracking strain option available in Abaqus Standard. The tension stress–strain data using the tension stiffening model of concrete proposed by Wahalathatri [43] was adopted in this study for unheated unconfined, post-heated unconfined and post-heated FRP confined concrete. Figure 5 shows the tensile stress–strain relationship used in the study for all temperatures and repair techniques used.

3.1.2 Reinforcing steel

Figure 6 shows the linear elastic and nonlinear plastic stress–strain relationship of reinforcing steel used in the model. The reinforcements in columns were arranged in such a way to maintain cover of 25 mm at both the tension face and the compression face of the column. The yield strength was determined at the 0.2% strain offset. The properties of reinforcing bars used in the model based on BS EN 1992-1-1 are shown in Table 8. The geometry adopted for samples is given in Figure 7.

3.2 Element type

An 8-node linear brick, reduced integration hourglass control solid element C3D8R (available in Abaqus Standard solid element library) was used to model the concrete. Three translational degrees of freedom at each node are present in C3D8R solid element. To avoid excessive stiffness due to shear locking effect and to improve the accuracy of results, a reduced integration was adapted. The longitudinal and transverse reinforcement was modeled using two-node linear 3-D truss elements called T3D2 available in Abaqus Standard library.

3.3 Finite element mesh

The assembled reinforced concrete column was then meshed by applying the structural meshing technique to the entire model. The precision of finite element analysis results depends on the selection of suitable mesh size to achieve both precision in results and not prolong the time for convergence. The different mesh sizes generally show slightly varying solutions. However, a very small mesh size takes a long time for convergence and makes the problem very complex increasing computational analysis time. In the present study, an optimum mesh size of 60 mm was adopted for truss elements based on the mesh convergence study. Figure 8(c) shows the meshing of modeled reinforced concrete columns. The same mesh size was adopted for meshing the solid brick elements type C3D8R and truss elements type T3D2. The full-size column was modeled with 8235 elements of type C3D8R. The total elements in the main reinforcement were 348 linear line elements of type T3D2 while total elements in transverse reinforcement were 198 linear line elements of type T3D2.

3.4 Interaction between concrete and reinforcement

The longitudinal and transverse reinforcement was embedded in the host solid element (the concrete part of the column) using the embedded element option (available in Abaqus Standard) as shown in Figure 8(a).

3.5 Boundary and loading conditions

To simulate the better experimental load–displacement behavior, two steel loading plates of very high stiffness were modeled, one at the top and the other at the bottom surface of the column, to apply the boundary conditions and eccentric uniform compression loading as shown in Figure 8(d). The bond between the steel loading plates and concrete was modeled using tie constraints. The load transferring surfaces (bottom surface of the top steel loading plate and the bottom surface of the concrete column) were assigned as master surface. However, the top surface of the concrete column and the top surface of the bottom steel plate was taken as the slave surface. The boundary condition applied in the full model axially loaded column was simulated as simple support (pin support). In this boundary condition, displacement in X, Y, Z directions was prevented. The bottom end of the columns was fixed in all directions using the boundary condition as encastre in Abaqus as shown in Figure 8(d). However, the top end of the columns was kept free in the direction of axial applied loading. An induced displacement of 25 mm was

applied through the top rigid steel loading plate as a uniformly distributed load on the top surface of the concrete columns. The displacement-controlled mode was adopted to determine the better post-peak load–displacement response of reinforced concrete columns. The loading increments, sizes in the step module of Abaqus, of minimum and maximum increment values were fixed in order to make the analysis faster.

3.6 Post-heated unconfined columns

The finite element modeling of post-heated unconfined concrete was carried out in similar steps as that of controlled samples. The model that was finalized for the unheated and unconfined reinforced concrete circular column was used for this technique also, with variation in material properties of concrete. The stress–strain curve used in the previous model was that of unheated and unconfined concrete; however, in this model, the stress–strain curves used were those of post-heated unconfined cylinders at 300°C, 500°C and 900°C. There are also some changes in the general properties of concrete as shown in Table 9, while the properties of the steel plate and steel reinforcement remained the same.

3.7 Post-heated CFRP confined

Different methodologies are used to model CFRP confined reinforced concrete columns. One of them is that part is created and different properties are defined, that feature is selected as shell, and the length and diameters are decided according to sample size. One of the major issues with this method is modulus of elasticity and Poisson's ratios are required in X, Y, Z planes. These properties cannot be found easily so this study used another approach, in which post-heated CFRP confined cylinders were tested. The experimental values of stress vs strain curves obtained for both tension and compression as shown in Figures 4 and 5 acted as input properties of concrete solid homogeneous in Abaqus. The general properties used for concrete are shown in Table 10.

3.8 Post-heated epoxy injected steel wire mesh covered CFRP confined reinforced concrete column

The modeling of this technique is also based on the properties obtained by experimental testing of post-heated cylinders repeated through epoxy injected steel wire mesh covered CFRP

confinement. The strain vs strain curve for compression as well as tension obtained by plotting experimental data is used as input as given in Figure 4 and Figure 5 respectively. The other properties of concrete used are shown in Table 11. The steps, properties of each part, assembly and interactions are repeated as for the controlled sample.

4. Regression models for prediction of axial load carrying capacity of columns

4.1 Post-heated unconfined reinforced circular columns

A simple linear regression model is developed for the reduction in strength of concrete after being subjected to heating. Simple linear regression model coefficients taken from SPSS (IBM) are used to predict residual axial capacity after heating. The performance of the simple linear regression model can be seen from the value of r^2, as 92.4% of the change in axial load capacity values can be explained by model input variables. There is a relatively high correlation coefficient 'R' of 96.1% between actual and predicted values. The significance value of 0.0093 is well below 0.05 (P < 0.05). The Root Means Square Error is 0.0243 which is very small and literature shows the smaller the value of the RMSE the better the model prediction. The performance measure parameters show an excellent curve fit model.

4.2 Post-heated CFRP confined reinforced circular columns

An effort is made to restore the reduction in the axial capacity of post-heated reinforced circular columns by applying CFRP confinement. As more than one independent variable of temperature, as well as the thickness of CFRP, played a role, multiple linear regression models were developed to predict the combined effect of heat and CFRP thickness on circular columns. To get a higher value of the coefficient of determination, capacity equations were developed at different ranges of temperature. An excellent curve fit was achieved with a coefficient of determination as well as a coefficient of correlation above 90%. The value of RMSE and significance were also within specified statistical guidelines.

4.3 Post-heated epoxy injected steel wire mesh, cement sand mortar covered and wrapped with CFRP

Post-heated columns were repaired with the injection of epoxy and covered with steel wire mesh. The opening of the wire mesh was filled with cement sand mortar and wrapped with CFRP sheet.

11

As more than one variable has an effect on axial capacity restoration, multiple regression models were developed involving the effect of temperature and thickness of layer constituted by epoxy injection wire mesh covering and CFRP wrap. Performance measures show that the mode has excellent correlations and more than 90% of the variation is explained by predicted multiple regression models with a very good sign. Results and minimum root-mean-square values which actually represent the difference of measured and predicted values.

4.4 Regression equations for the prediction of axial deformation capacities

The load vs deformation curve plotted for experimental values of post-heated unconfined samples showed a quadratic relationship. A quadratic regression model was developed to predict axial deformation of unconfined post-heated reinforced circular columns, with deformation as dependent and load as an independent variable. However, it is noted that the relationship is not valid for the whole range of temperature for which the axial capacity prediction equation is developed so the range is applied to the model constructed. In the case of carbon fiber reinforced polymer confined post-heated circular columns subjected to axial loading, due to the higher value of deformation after confinement, the equation has a large value of Y-intercept showing that the model will predict higher deformations as the best fit curve. However, slight variation may be noted during small values. The quadratic regression relation is constituted in the form of the following equations. The deformation prediction equations are also developed for post-heated epoxy injected steel wire mesh, cement sand mortar covered wrapped with CFRP (PH-EF-WM-CSM-CFRP) to make quick and reliable predictions. The deformation prediction models for epoxy injected steel wire mesh covered with an opening covered with cement sand mortar and wrapped with CFRP had the best-fit curve of all the models. The load vs deformation curves plotted for the experimental, quadratic regression model and finite element model are very close reflecting an excellent result. The high value of the coefficient of determination R^2 for models at all three temperatures shows that more than 90% of the axial deformation values can be explained by model input variables. The correlation coefficient R also supports the same interpretation. The lower values of means square error and within limit results of significance at all temperatures support the model which gives the best curve fit and can best predict the values of axial deformation of post-heated circular columns at any temperature.

12

5. Comparison of results obtained from experiments, numerical models and regression equations

5.1 Axial load capacity

The average experimental values of axial load capacity recorded for controlled unheated unconfined (UH-UC) samples are 1353 kN and those obtained by using the regression equation and finite element model are 1320 kN and 1365 kN, respectively. The percentage difference calculated for controlled samples is -0.83% in the finite element model and 2.43% in the regression model. The percentage difference shown by the regression equation is relatively greater than that by finite element model because regression analysis provides a perfectly clear relationship between explanatory variables and dependent variables. The regression equations developed for different repair techniques and heating conditions are stated below.

$$P_{n\theta} = -0.6793\theta + 1.042 \, (0.85fc' \, (A_g - A_{st}) + f_y A_{st}) \qquad (100°C \leq \theta \leq 900°C)$$

$P_{n\theta}$ is the value of residual axial load capacity (kN) of post-heated unconfined reinforced circular columns and "Θ" represents the value of temperature in degrees Celsius.

$$P_{ntf\theta} = 147.69t_f - 0.77\theta + 1.426(0.85fc'(A_g - A_{st}) + f_y A_{st}) \quad (100°C \leq \theta \leq 900°C)$$

$P_{ntf\theta}$ shows the confined load capacity of post-heated CFRP confined reinforced circular columns in kN at particular values of thickness and temperature, Θ represents temperature in degrees Celsius and t_f is the symbol used for the thickness of CFRP fiber in mm.

$$P_{nec\theta} = 47.69t_f - 0.89\theta + 1.426(0.85fc'(A_g - A_{st}) + f_y A_{st}) \qquad (100°C \leq \theta \leq 900°C)$$

$P_{nec\theta}$ represents the axial load capacity of post-heated epoxy injected steel wire mesh covered CFRP confined in kN, t_f is the thickness of the layer in mm constituted by a combination of above-stated materials and Θ is the temperature in degrees Celsius. Reduction in axial load capacity is noted after subjecting the samples to heat. Post-heated (300°C) unconfined axial load capacity is 12% less than for unheated unconfined columns. This is caused by the high temperatures driving out of moisture and concrete hydration. An effort is being made to restore the reduction in axial load caring capacity. CFRP confinement is applied to damaged reinforced circular columns. CFRP increased the axial capacity of the damaged reinforced circular column by 79.8% more than the controlled sample because when the concrete is fully cracked the activated CFRP confinement provides additional load carrying capacity by keeping the concrete

core intact. The values predicted by numerical and regression modeling for both post-heated (300°C) unconfined and post-heated (300°C) CFRP confined lie close to the experimental values. The percentage difference between numerical and regression values is -0.74% and 0.25% for the unconfined and confined, respectively.

The use of CFRP confinement to repair the damaged column solved the problem of restoring axial load carrying capacity but had no significant effect on the value of stiffness because the use of CFRP resulted in increased deformation. For the stated reason, it was decided to use such a technique to increase not only axial load capacity but also the stiffness of members, so that load can be transferred efficiently. Epoxy injected steel wire mesh covered and CFRP wrapping was used for this purpose. This resulted in a significant increase in axial capacity (100%) and also controlled deformation, thus providing adequate stiffness to the member to pass load safely. The percentage difference of predicted values using the above-stated equation and the finite element model for all techniques is less than 3%. The positive sign for percentage difference shows that the predicted values of the finite element model are slightly higher than the experimental results. The CFRP wrapped and epoxy injected steel wire mesh covered and CFRP wrapped models are very complex. Table 12 summarizes the increase and decrease in load carrying capacity at 300°C, repaired and using different repair techniques and percentage difference of recorded and predicted values. Graphical relationships are shown in Figure 9.

This procedure was repeated for 500°C and 900°C. The axial capacity of post-heated 500°C unconfined reinforced circular columns was reduced by 27% after being subjected to heating. CFRP confinement used as a repair technique increased axial capacity by 60% more than that of the controlled sample. It is important to note that this increase in strength for CFRP confined samples was 120% more than the post-heated 500°C unconfined case. However, confinement had no effect on stiffness that had been considerably reduced by heating. To solve this problem, the epoxy fill wire mesh covered CFRP confined technique was used which not only increased the strength by 80% more than the controlled sample strength but also solved the stiffness issue.

The values of axial capacity predicted by using regression and finite element models are given in Table 13. In particular, the finite element analysis results seemed to correlate well with

corresponding experimental data. The percentage differences of predicted values by both models from the experimental values are less than 5% with the only exception of the finite element model for post-heated 500°C unconfined reinforced circular columns where about 8% difference exists. The negative sign in the table shows values are overestimated. The graphical comparison of axial load capacity at 500°C by using different repair techniques is shown in Figure 10. Similarly, when subjected to 900°C the reinforced circular columns lost about 47% of axial capacity. The use of CFRP increased strength by 30% more than that of the controlled sample. Epoxy injected steel wire mesh covered CFRP confined improved strength by almost 50% (48.5%). It is worth mentioning that CFRP had a 147% increase and use of epoxy injection steel wire mesh and CFRP confinement had a 184% increase compared to post-heated 900°C unconfined samples.

The predictions made by using regression and finite element models are given in Table 14. The overestimated values are represented by a negative sign. Results show that the finite element model slightly over predicts the axial capacity. The percentage difference of the regression and finite element models to the experimental values are within specified limits except for post-heated 900°C unconfined which overestimates by about 9%. The graphical relationship for post-heated 900°C using a different repair technique is shown in Figure 11. A regression model represents enactment in ideal conditions; even imitation shows performance in ideal conditions.

5.2 Axial deformation

The axial deformation of the column increases after being subjected to heat. Taking into account the effect of repair techniques on the deformation of the damaged reinforced circular column, it is noted that deformation increases with CFRP confinement. The use of epoxy filled steel wire mesh covered CFRP confinement resulted in controlled deformation. The results obtained for axial deformation of unheated unconfined, post-heated (300°C) unconfined, post-heated (300°C) CFRP confined and post-heated (300°C) epoxy injected wire mesh covered CFRP confined columns by using the regression model is very close to the experimental values. However, due to higher values of deformation, the regression model equations of post-heated unconfined and post-heated CFRP confinement have high values of Y-intercept. Because of this, the relationship developed by the regression model cannot predict good values of deformation at lower load. The

equations developed to predict the value of axial deformations are stated in Table 18. The finite element model has resulted in excellent deformation prediction results. The load–deformation curves shown in Figures 12–15 follow the same trend as the experimental values. The experimental, regression and finite element model comparisons for deformation prediction and percentage difference are shown in Table 15. The comparison of maximum deformation for each technique is plotted in Figure 22. The analytical discussion provides a clearer picture of the approach used in different scenarios.

Similar to the samples subjected to 300°C, the deformation of post-heated 500°C unconfined columns increased after being subjected to such a high temperature. The predictions made by the regression and Abaqus models are very close to the experimental values. The overestimated values are represented by the negative signs. Excellent predictions are made by both models (regression and finite element model) except the regression model for post-heated 500°C CFRP confined reinforced circular columns that shows 8% underestimation as reported in Table 16. The prediction equations showed that because of the y-intercept in the relationship developed, the results for small values of deformation and load may not be predicted well. However, best-fit curves are predicted for higher loads as shown in Figures 16–21. The comparison of maximum deformation for each repair technique for the stated temperature is shown in Figure 23. The deformation of reinforced circular columns increased by more than 200%, 600% and 173% for post-heated (900°C) unconfined, post-heated (900°C) CFRP confined and post-heated (900°C) epoxy injected wire mesh covered CFRP confined columns respectively. Moreover, the predicted values of regression and finite element models showed close results to the experimental deformations. The predicted values of models for all repair techniques and their percentage differences with experimental values are presented in Table 17. Just like the previous cases, the deformation curve plotted does not follow a trend for small values of load and deformation, however this problem is avoided for large deformations under heavy loads as shown in Figures 20 and 21. The comparison of maximum deformations for the full set of repair techniques at 900°C is also shown graphically in Figure 24. It is easy to design, repeat and statistically analyze the computer-generated results; however, they do not provide a depiction that is as accurate as analytical models. The advantage is to find initial results quickly and do rapid prototyping, which gives feedback on the design of procedures. Mathematical or analytical proof requires abstraction, which is an important issue.

6. Conclusion

The following conclusions can be drawn based on the results of the present study.

1. The prediction of axial load capacity by finite element analysis and regression equations confirmed the experimental results that subjecting reinforced circular columns to high temperatures of 300°C, 500°C and 900°C reduced axial load capacity by 12%, 27% and 48% respectively and increased deformation.

2. Models confirmed that CFRP confinement not only increased the axial load capacity but also the deformations, thus causing a reduction in stiffness.

3. Epoxy injected, steel wire mesh-covered CFRP confinement increased the axial load capacity and controlled deformations. Thus, it can be declared as the best technique for the repair of fire-damaged concrete structures.

4. The values of axial load capacity predicted by regression models for post-heated (300°C, 500°C and 900°C) unconfined columns and post-heated (300°C, 500°C and 900°C) columns repaired using advanced material shows excellent fit models. The percentage differences between predicted values and experimental values are well below 10% for all temperatures and repair techniques showing excellent results. This confirms that these equations can be adopted for quick and reliable predictions.

5. The predicted results from the deformation equations showed high precision at higher loads while the results for lower values of load are not as precisely predicted because of the Y-intercept in the equation. Thus, these equations can be used to predict deformations at higher load only.

6. Finite element models predicted values for all sets of temperatures and repair techniques which also showed minor differences with experimental values of less than 8% for all temperature and repair methods.

This study concludes that prediction equations and finite element analysis offer a promising alternative to experimental methods which are expensive and time consuming and often limit the pace of research progress. Moreover, existing structures cannot be tested at ultimate failure because of limitations of equipment, and scale effects on large structures cannot be observed experimentally. These constraints have strongly encouraged the development of advanced numerical and analytical methods capable of representing the behavior of concrete structures reinstated by composite materials under all possible loading conditions.

Acknowledgments

References

[1]   R. A. B. O. FIRE-DAMAGED, "RESILIENT INFRASTRUCTURE," 2016.

[2]   M. Yaqub and C. Bailey, "Repair of fire damaged circular reinforced concrete columns with FRP composites," *Construction and Building Materials,* vol. 25, pp. 359-370, 2011.

[3]   H. Al-Nimry, R. Haddad, S. Afram, and M. Abdel-Halim, "Effectiveness of advanced composites in repairing heat-damaged RC columns," *Materials and Structures,* vol. 46, pp. 1843-1860, 2013.

[4]   M. Yaqub, C. Bailey, P. Nedwell, Q. Khan, and I. Javed, "Strength and stiffness of post-heated columns repaired with ferrocement and fibre reinforced polymer jackets," *Composites Part B: Engineering,* vol. 44, pp. 200-211, 2013.

[5]   M. Yaqub and C. Bailey, "Cross sectional shape effects on the performance of post-heated reinforced concrete columns wrapped with FRP composites," *Composite Structures,* vol. 93, pp. 1103-1117, 2011.

[6]   E. U. Chowdhury, L. A. Bisby, M. F. Green, and V. K. Kodur, "Investigation of insulated FRP-wrapped reinforced concrete columns in fire," *Fire Safety Journal,* vol. 42, pp. 452-460, 2007.

[7]   M. Yaqub and C. Bailey, "Seismic performance of shear critical post-heated reinforced concrete square columns wrapped with FRP composites," *Construction and Building Materials,* vol. 34, pp. 457-469, 2012.

[8]   M. F. M. Zain, S. Abd, K. Sopian, M. Jamil, and A. Che-Ani, *Mathematical regression model for the prediction of concrete strength*, 2008.

[9]   M. F. M. Zain and S. M. Abd, "Multiple regression model for compressive strength prediction of high performance concrete," *Journal of Applied Sciences,* vol. 9, pp. 155-160, 2009.

[10]   P. Chopra, R. Sharma, and M. Kumar, "Regression models for the prediction of compressive strength of concrete with & without fly ash," *International Journal of Latest Trends in Engineering and Technology (IJLTET),* vol. 3, pp. 400-406, 2014.

[11]   U. Atici, "Prediction of the strength of mineral admixture concrete using multivariable regression analysis and an artificial neural network," *Expert Systems with Applications,* vol. 38, pp. 9609-9618, 2011.

[12]   A. Aljanabi, *Finite Element Modeling of Reinforced Concrete Column after Exposure to Fire* vol. 3, 2017.

[13]   D. Hu and M. Barbato, "Simple and efficient finite element modeling of reinforced concrete columns confined with fiber-reinforced polymers," *Engineering Structures,* vol. 72, pp. 113-122, 2014.

[14]   S. Chaudhari and M. Chakrabarti, "Modeling of concrete for nonlinear analysis using finite element code ABAQUS," *International Journal of Computer Applications,* vol. 44, pp. 14-18, 2012.

[15] P. Sadeghian, A. Rahai, and M. Ehsani, *Numerical Modeling of Concrete Cylinders Confined with CFRP Composites* vol. 27, 2008.

[16] Y. S. Al-Kamaki, R. Al-Mahaidi, and I. Bennetts, "Experimental and numerical study of the behaviour of heat-damaged RC circular columns confined with CFRP fabric," *Composite Structures,* vol. 133, pp. 679-690, 2015.

[17] M. Chellapandian, S. S. Prakash, and A. Rajagopal, "Analytical and finite element studies on hybrid FRP strengthened RC column elements under axial and eccentric compression," *Composite Structures,* vol. 184, pp. 234-248, 2018.

[18] M. M. Bikhiet, N. F. El-Shafey, and H. M. El-Hashimy, "Behavior of reinforced concrete short columns exposed to fire," *Alexandria Engineering Journal,* vol. 53, pp. 643-653, 2014.

[19] Y. Tao and J.-F. Chen, "Concrete damage plasticity model for modeling FRP-to-concrete bond behavior," *Journal of Composites for Construction,* vol. 19, p. 04014026, 2014.

[20] B. Piscesa, M. M. Attard, and A. K. Samani, "Three-dimensional finite element analysis of circular reinforced concrete column confined with FRP using plasticity model," *Procedia Engineering,* vol. 171, pp. 847-856, 2017.

[21] T. Yu, J. Teng, Y. Wong, and S. Dong, "Finite element modeling of confined concrete-II: Plastic-damage model," *Engineering Structures,* vol. 32, pp. 680-691, 2010.

[22] M. Z. Kabir and E. Shafei, "Plasticity modeling of FRP-confined circular reinforced concrete columns subjected to eccentric axial loading," *Composites Part B: Engineering,* vol. 43, pp. 3497-3506, 2012.

[23] S. Bratina, B. Čas, M. Saje, and I. Planinc, "Numerical modelling of behaviour of reinforced concrete columns in fire and comparison with Eurocode 2," *International Journal of Solids and Structures,* vol. 42, pp. 5715-5733, 2005.

[24] B. Alfarah, F. López-Almansa, and S. Oller, "New methodology for calculating damage variables evolution in plastic damage model for RC structures," *Engineering Structures,* vol. 132, pp. 70-86, 2017.

[25] A. Mosallam, K. Allam, and M. Salama, "Analytical and numerical modeling of RC beam-column joints retrofitted with FRP laminates and hybrid composite connectors," *Composite Structures,* vol. 214, pp. 486-503, 2019.

[26] I. Ciesielska-Wrobel, *Finite Element Modeling of Textiles in Abaqus™ CAE*: CRC Press, 2019.

[27] N. Wahid, T. Stratford, and L. Bisby, "Calibration of concrete damage plasticity model parameters for high temperature modelling of reinforced concrete flat slabs in fire," *Applications of Structural Fire Engineering 2019, Singapore,* 2019.

[28] B.-b. Li, H.-b. Xiong, J.-f. Jiang, and Y. Zhan, "Damage plasticity model for passively confined concrete," in *MATEC Web of Conferences*, 2019, p. 02016.

[29] A. Wosatko, A. Winnicki, M. A. Polak, and J. Pamin, "Role of dilatancy angle in plasticity-based models of concrete," *Archives of Civil and Mechanical Engineering,* vol. 19, pp. 1268-1283, 2019.

[30]   I. Hussain, M. Yaqub, A. Ehsan, and S. U. Rehman, "Effect of viscosity parameter on numerical simulation of fire damaged concrete columns," *Civil Engineering Journal,* vol. 5, pp. 1841-1849, 2019.

[31]   M. K. P. Kmiecik, "Modelling of reinforced concrete structures and composite structures with concrete strength degradation taken into consideration," *Archives of Civil and Mechanical Engineering,* vol. 11, pp. 623-636, 2011.

[32]   S. Al-Amin and R. Ahsan, "Finite element modeling of reinforced concrete column under monotonic lateral loads," *International Journal of Computer Applications,* vol. 42, pp. 53-58, 2012.

[33]   N. Halim, S. C. Alih, and M. Vafaei, "Structural behavior of RC columns transversely reinforced with FRP strips," *International Journal of Civil Engineering and Technology,* vol. 9, 2018.

[34]   E. Ellobody and C. G. Bailey, "Modelling of unbonded post-tensioned concrete slabs under fire conditions," *Fire Safety Journal,* vol. 44, pp. 159-167, 2009.

[35]   A. Raza and A. Ahmad, "Numerical investigation of load-carrying capacity of GFRP-reinforced rectangular concrete members using CDP model in ABAQUS," *Advances in Civil Engineering,* vol. 2019, 2019.

[36]   Y.-F. Chang, Y.-H. Chen, M.-S. Sheu, and G. C. Yao, "Residual stress–strain relationship for concrete after exposure to high temperatures," *Cement and Concrete Research,* vol. 36, pp. 1999-2005, 2006.

[37]   A. W. Beeby and R. Narayanan, *Designers' Guide to EN 1992-1-1 and EN 1992-1-2. Eurocode 2: Design of Concrete Structures: General Rules and Rules for Buildings and Structural Fire Design*: Thomas Telford, 2005.

[38]   Z. Ismail, S. Doostdar, and Z. Harun, "Factors influencing the implementation of a safety management system for construction sites," *Safety Science,* vol. 50, pp. 418-423, 2012.

[39]   K. K. B. a. M. R. M.K. Kassir, "Thermal degradation of concrete in the temperature range from ambient to 315°C", United States Department of Emergency report, Washington D.C October, 1996.

[40]   Eurocode-4, "Design of composite steel and concrete structures-Part 1-2; General rules-structural fire design" *BS EN 1994-1-2,* 2005.

[41]   J. B. Mander, M. J. Priestley, and R. Park, "Theoretical stress-strain model for confined concrete," *Journal of Structural Engineering,* vol. 114, pp. 1804-1826, 1988.

[42]   C. E. Bakis, A. Ganjehlou, D. I. Kachlakev, M. Schupack, P. Balaguru, D. J. Gee*, et al.*, "Guide for the design and construction of externally bonded FRP systems for strengthening concrete structures," *Report by ACI Committee,* vol. 440, 2002.

[43]   B. L. Wahalathantri, D. Thambiratnam, T. Chan, and S. Fawzia, "A material model for flexural crack simulation in reinforced concrete elements using ABAQUS," in *Proceedings of the First International Conference on Engineering, Designing and Developing the Built Environment for Sustainable Wellbeing*, 2011, pp. 260-264.

[44] A. C. Cameron and F. A. Windmeijer, "An R-squared measure of goodness of fit for some common nonlinear regression models," *Journal of Econometrics,* vol. 77, pp. 329-342, 1997.

[45] W. R. Rice, "Analyzing tables of statistical tests," *Evolution,* vol. 43, pp. 223-225, 1989.

[46] T. Chai and R. R. Draxler, "Root mean square error (RMSE) or mean absolute error (MAE)?–Arguments against avoiding RMSE in the literature," *Geoscientific Model Development,* vol. 7, pp. 1247-1250, 2014.

Figures

Figure 1: Heating of columns in the furnace
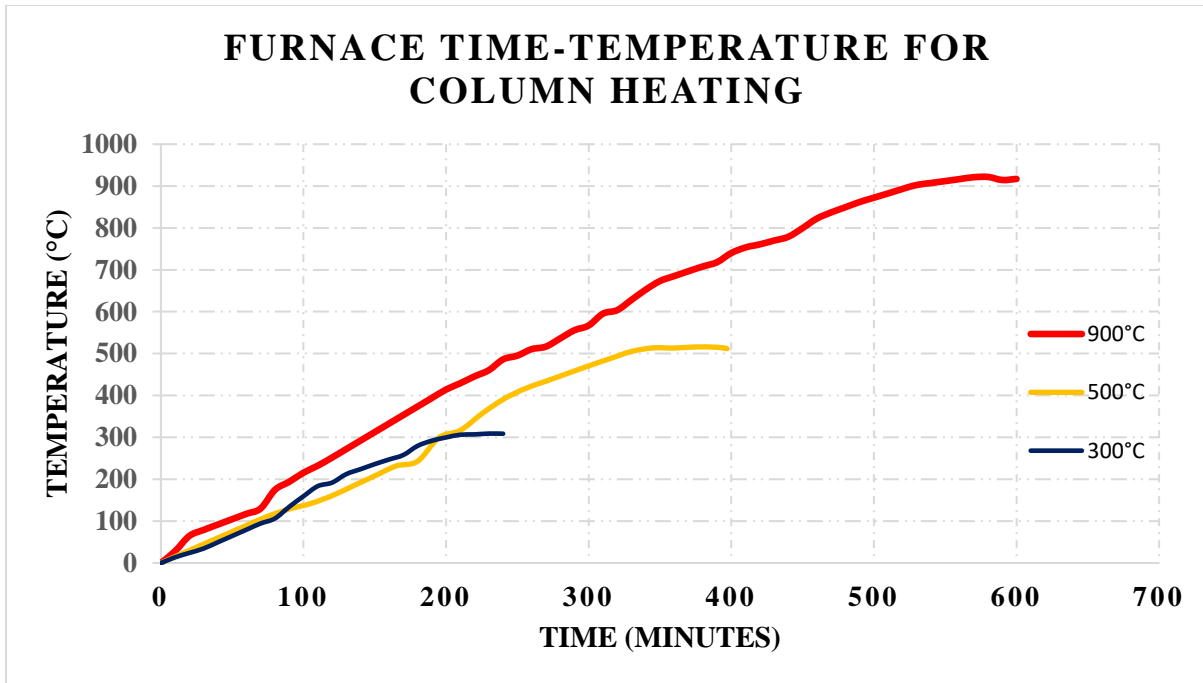
Figure 2: Time–temperature curve for heating of column specimens in furnace
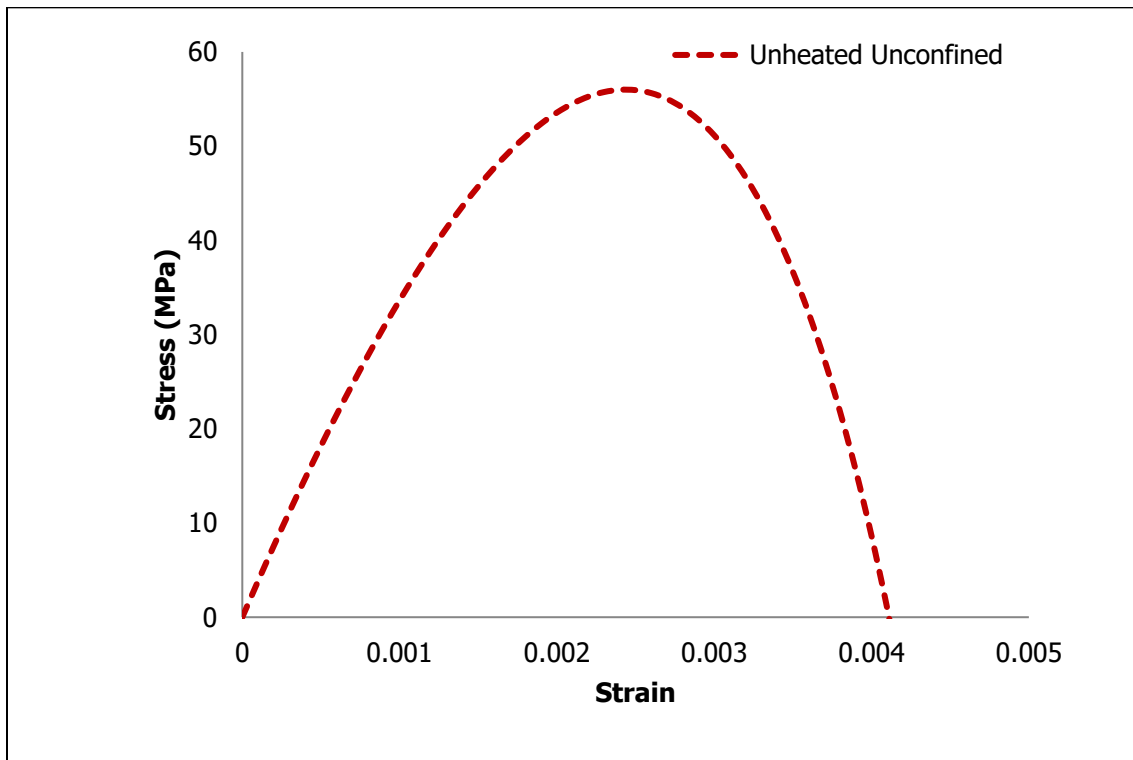
Figure 1: Stress–strain relationship for unheated and unconfined concrete in compression
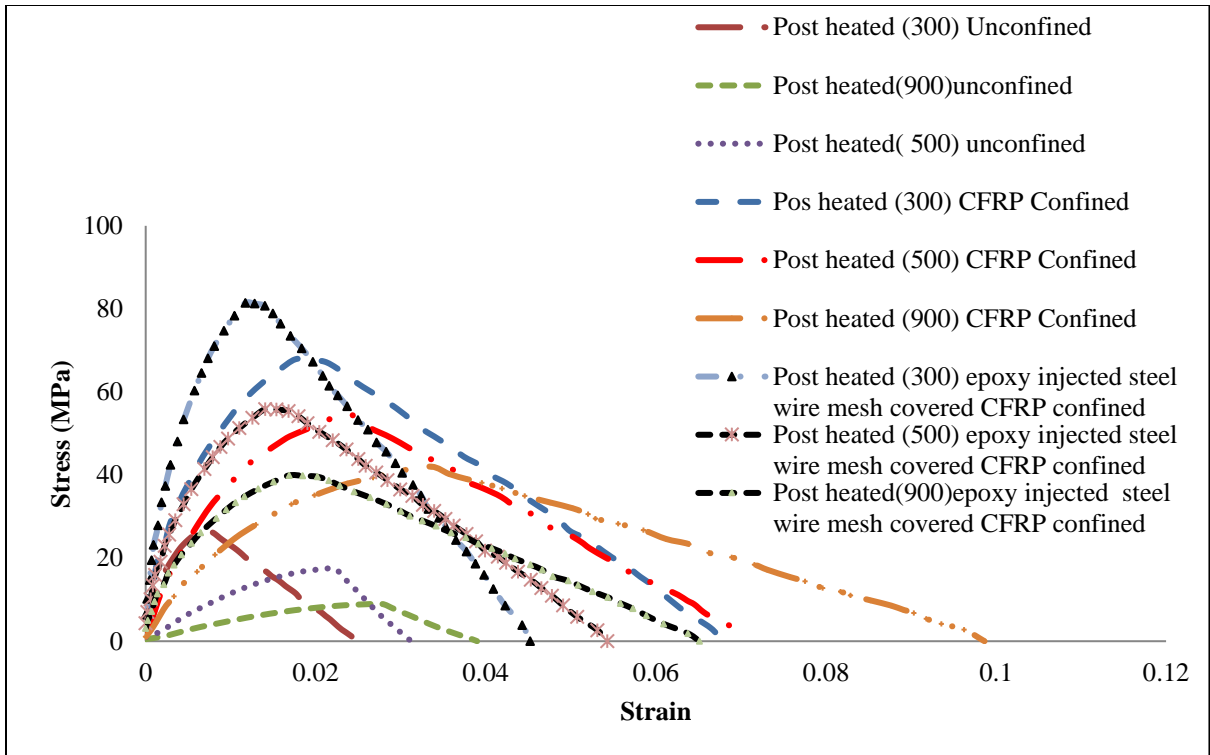
Figure 2: Stress–strain curves for post-heated (°C) repair techniques in compression
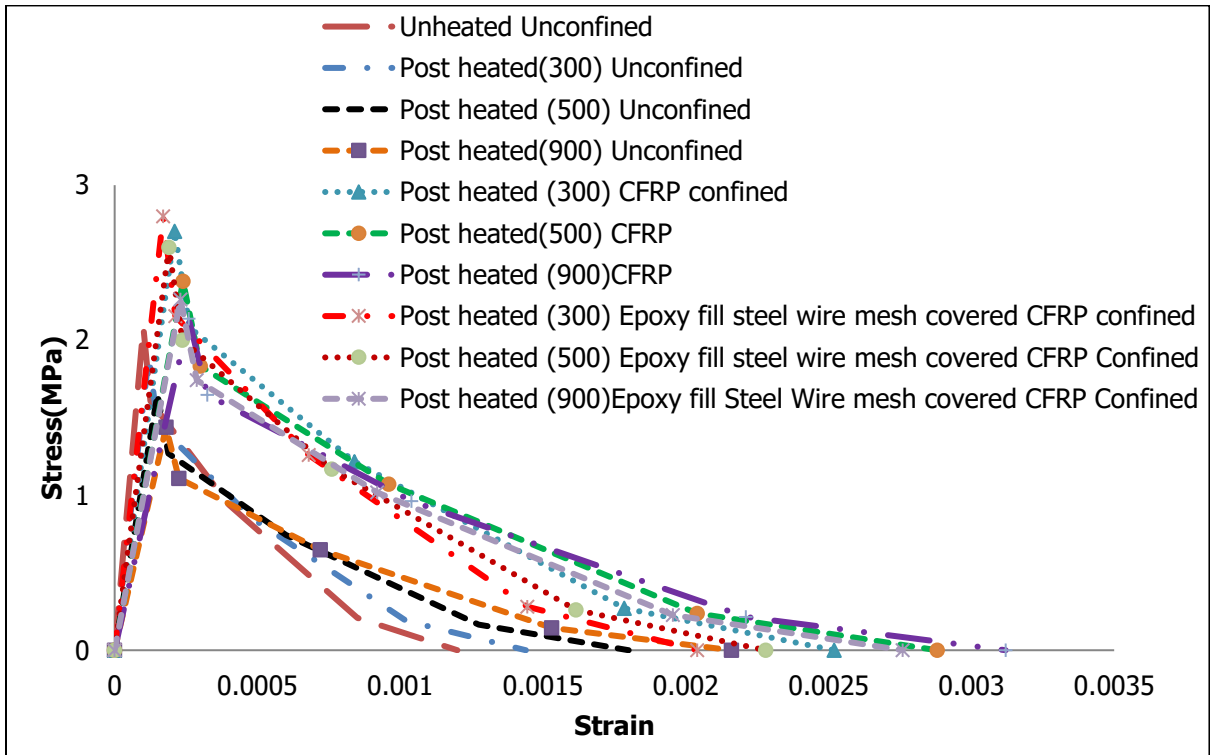
Figure 3: Stress–strain curves for post-heated (°C) repair techniques in tension
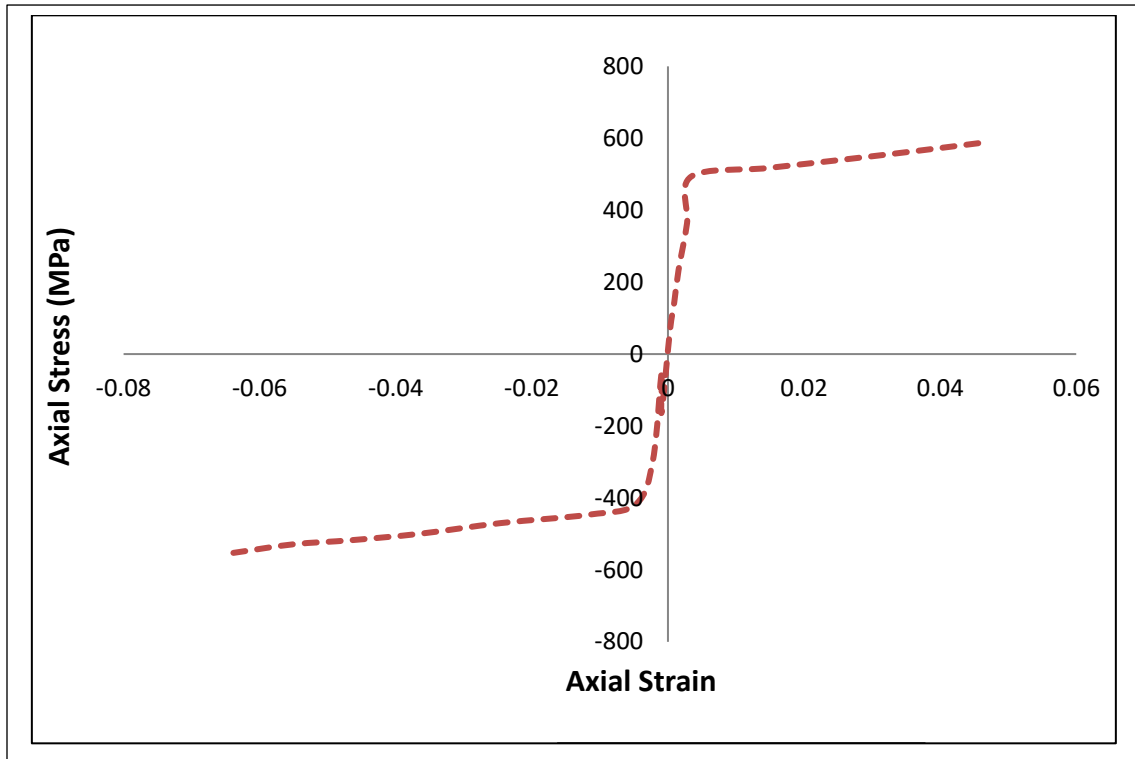
Figure 4: Bilinear stress–strain behavior of steel bars
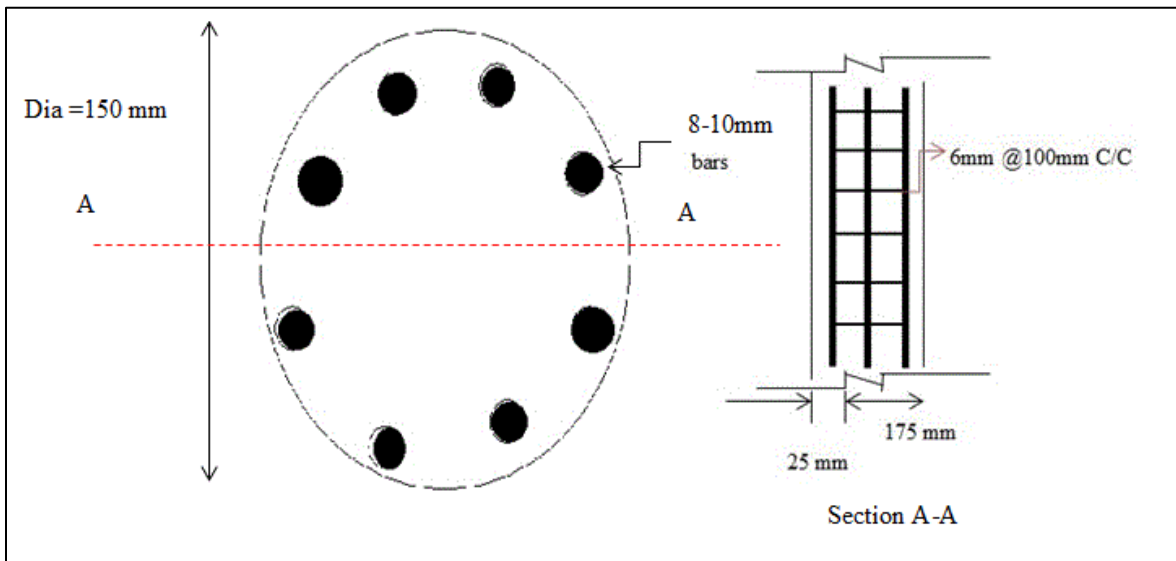
Figure 5: Details of reinforcement and the spacing
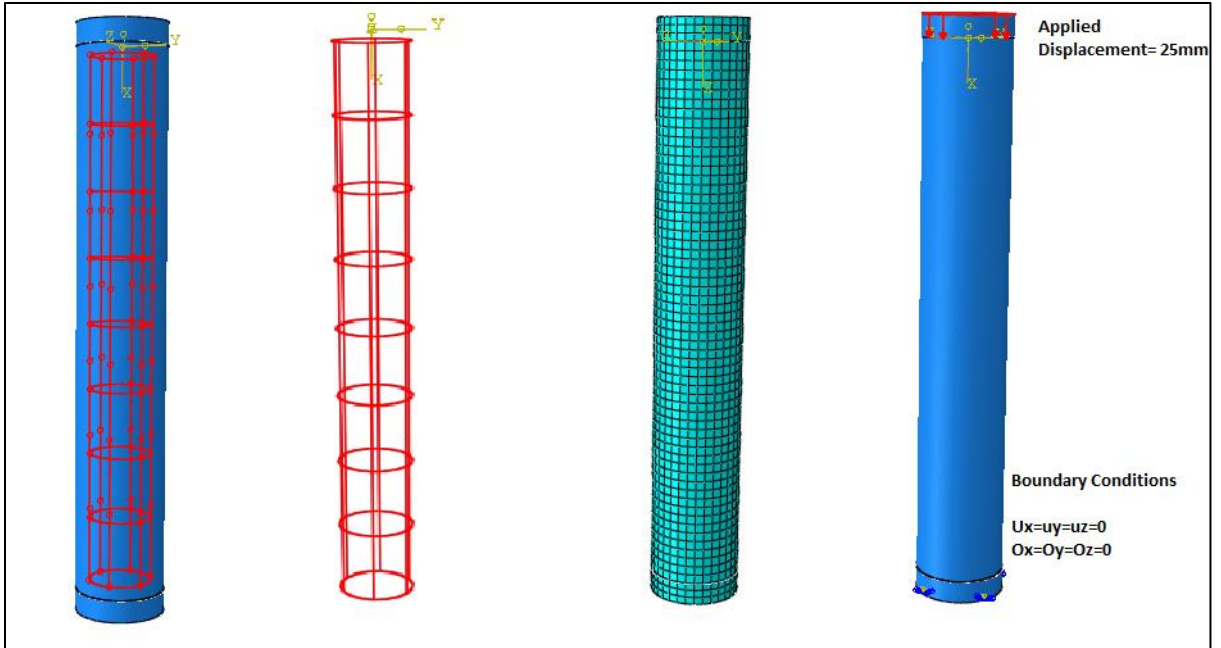
Figure 6: Abaqus model of column: (a) reinforcement embedded in concrete, (b) reinforcement, (c) finite element mesh, (d) boundary conditions
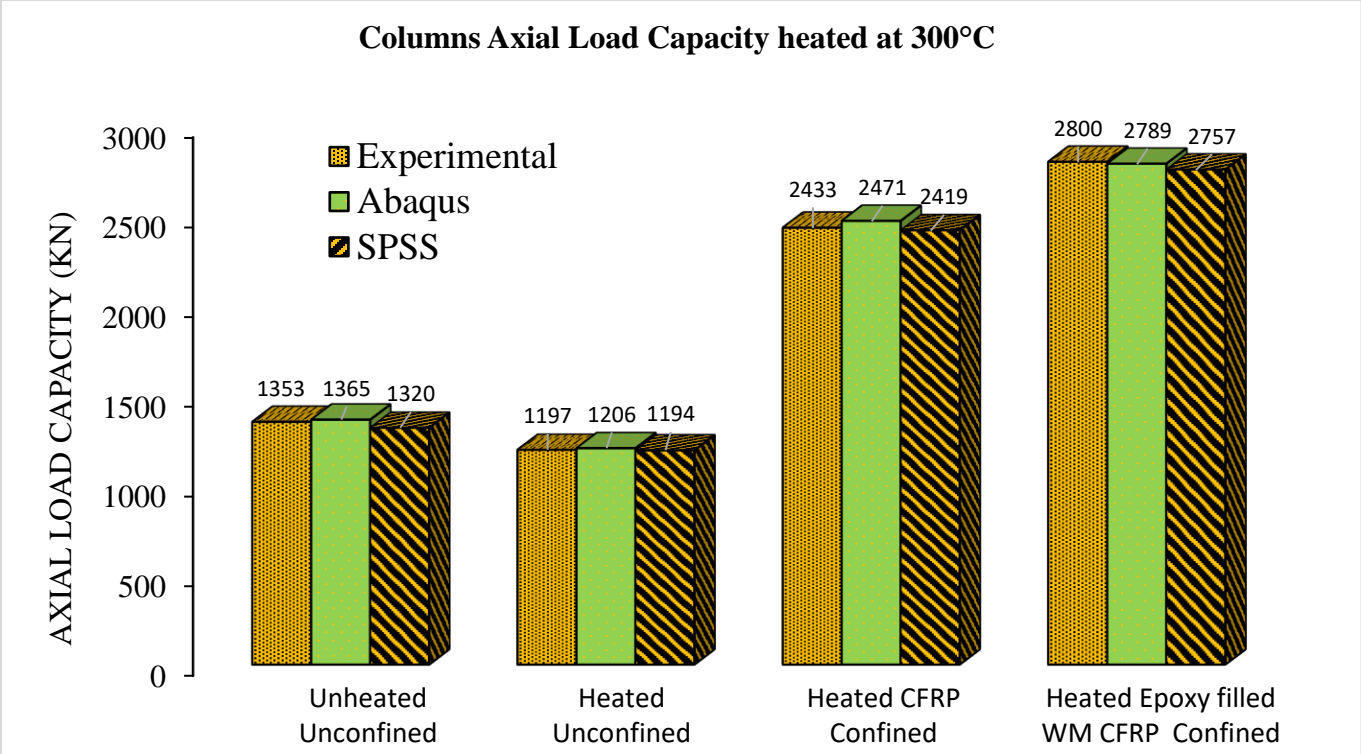
Figure 7: Axial load capacity comparison for post-heated 300°C columns
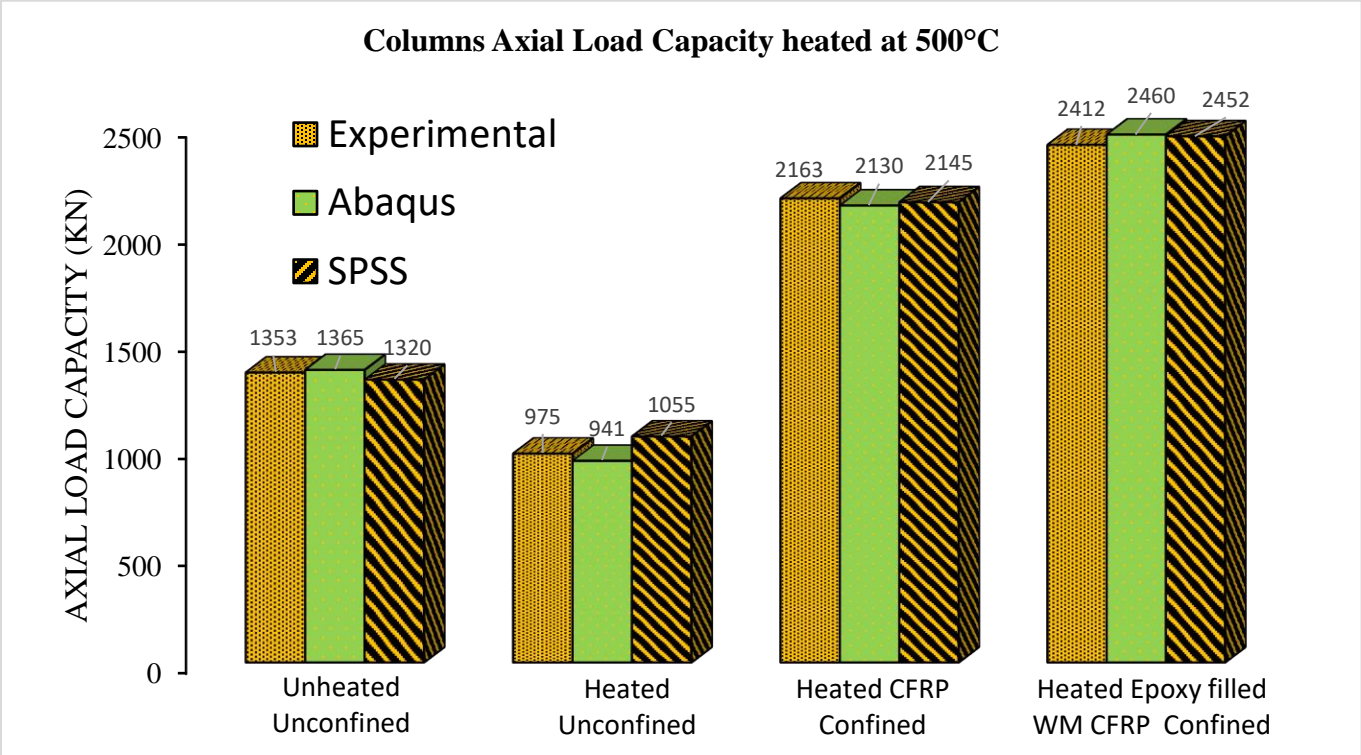
Figure 8: Axial load capacity comparison for post-heated 500°C columns
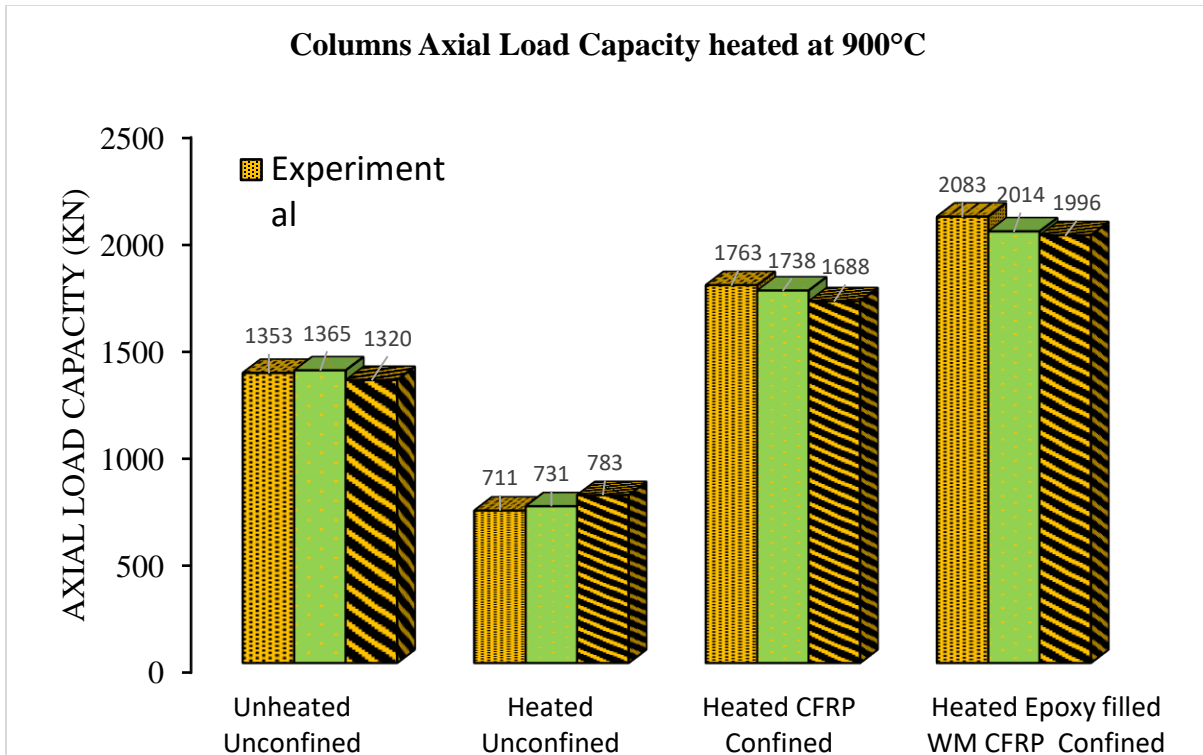
Figure 9: Axial load capacity comparison for post-heated 900°C columns
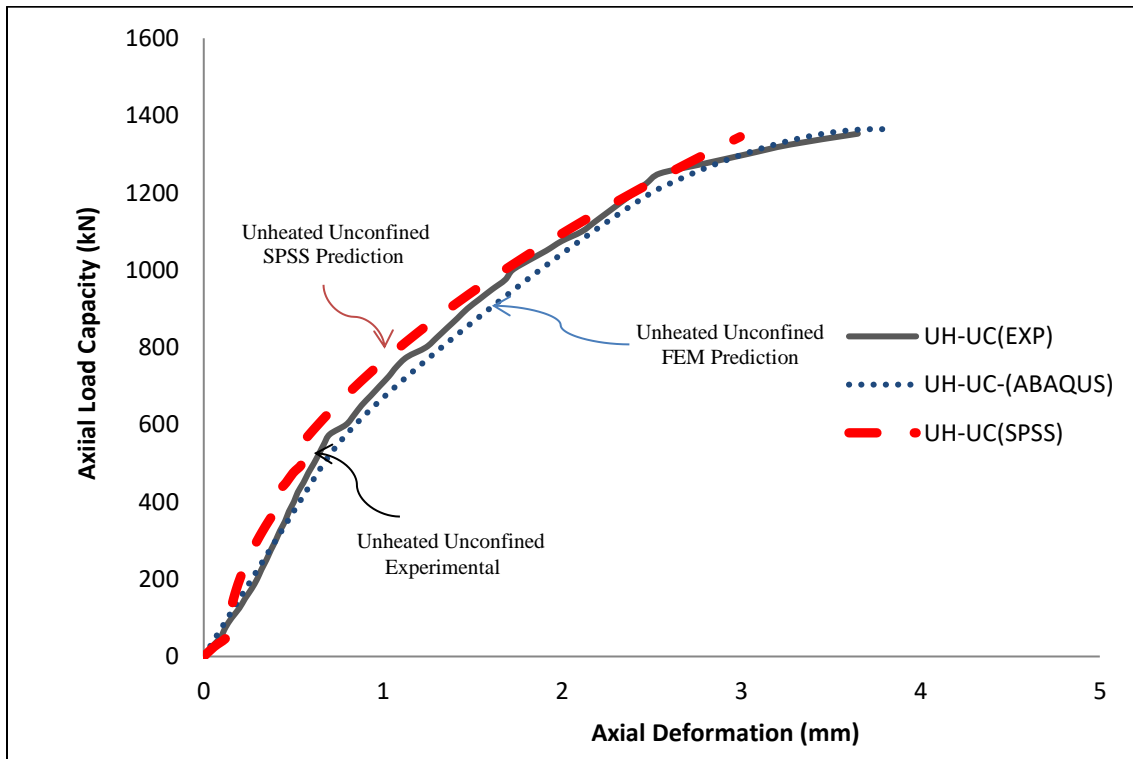
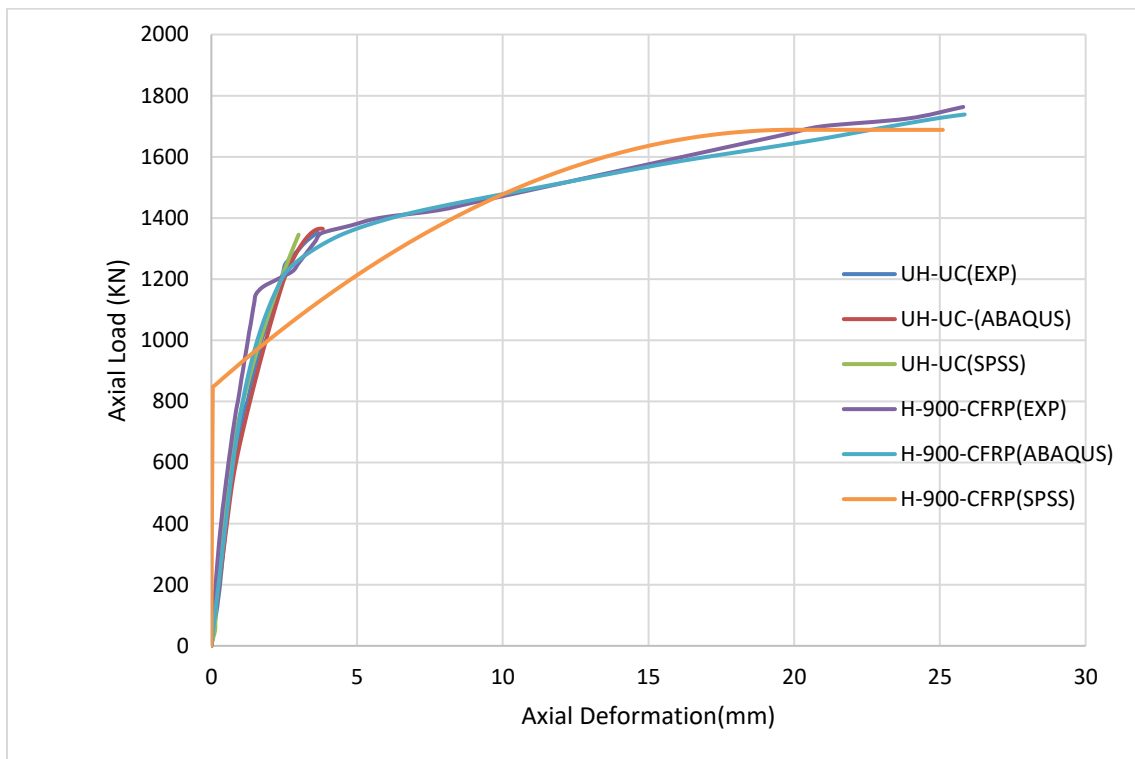Figure 10: Load vs axial deformation for unheated unconfined columns
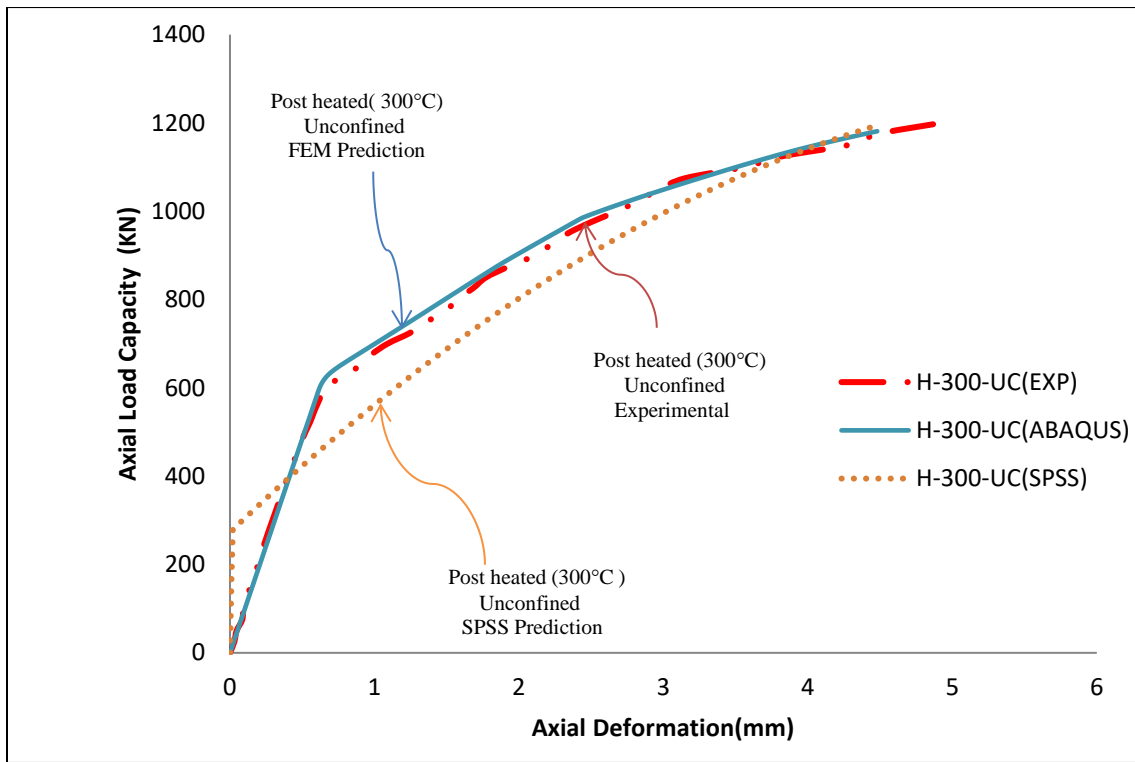
Figure 11: Load vs axial deformation for post-heated (300°C) unconfined column
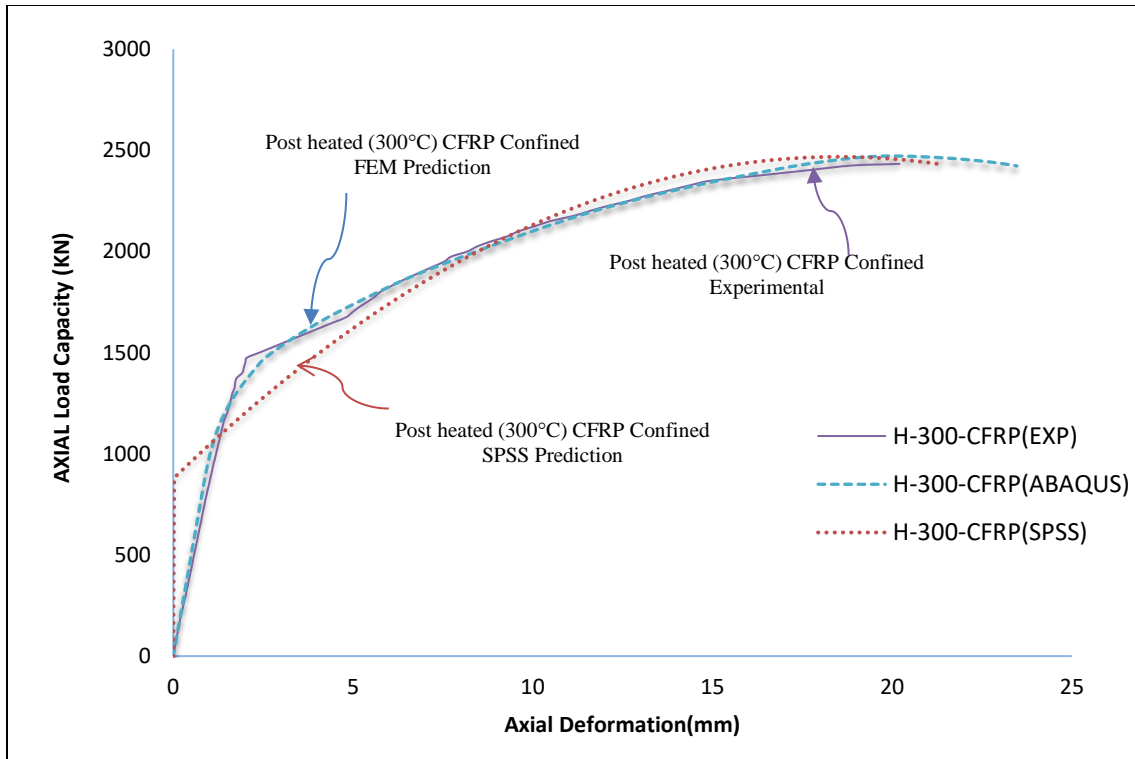
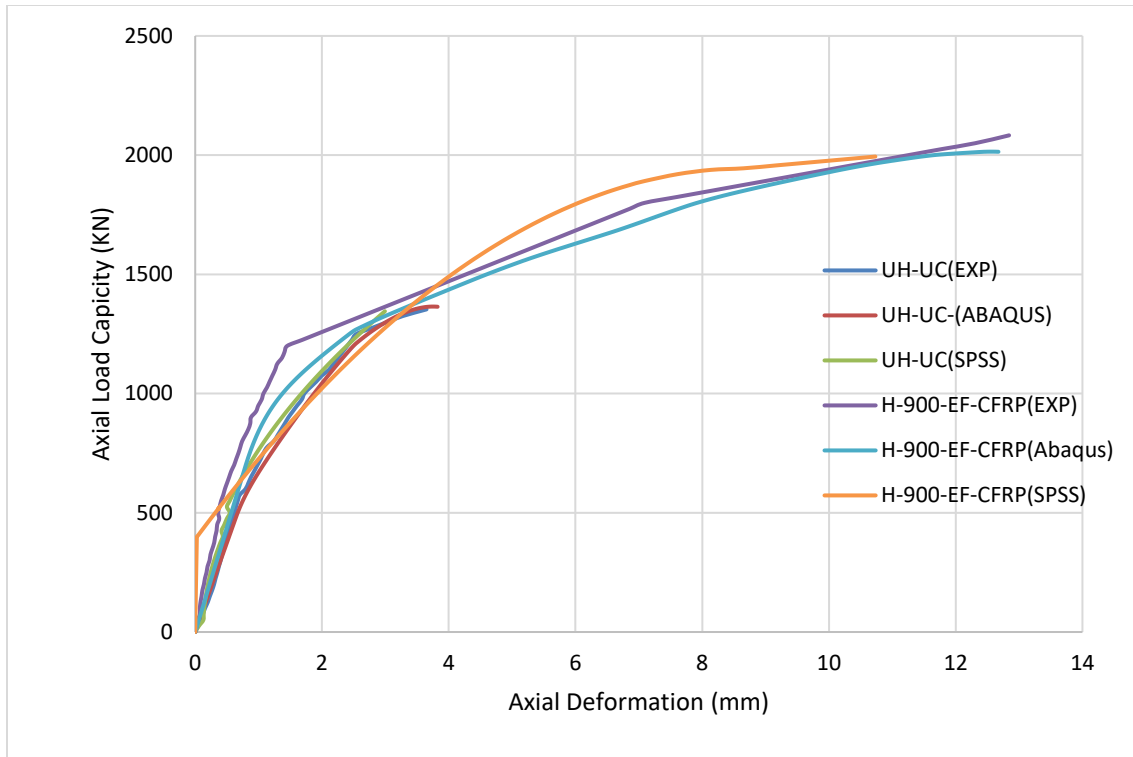Figure 12: Load vs axial deformation for post-heated (300°C) CFRP confined column
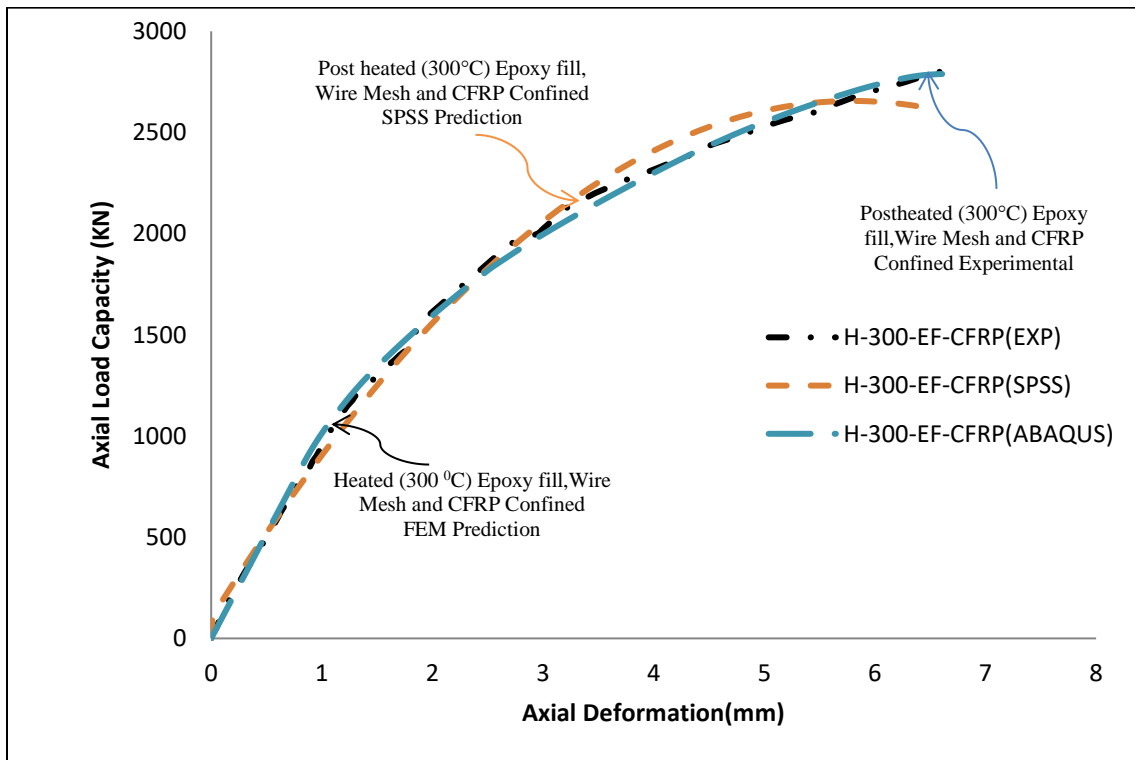
Figure 13: Load vs axial deformation for post-heated (300°C) epoxy fill steel wire mesh covered CFRP confined column
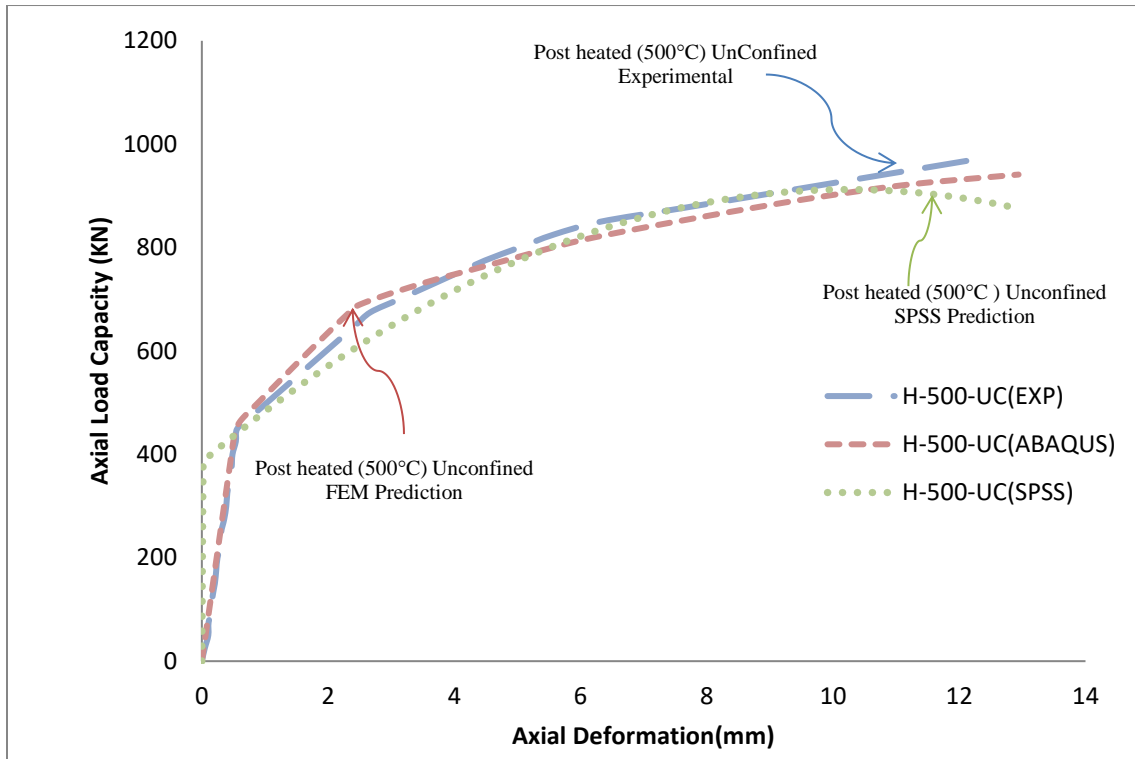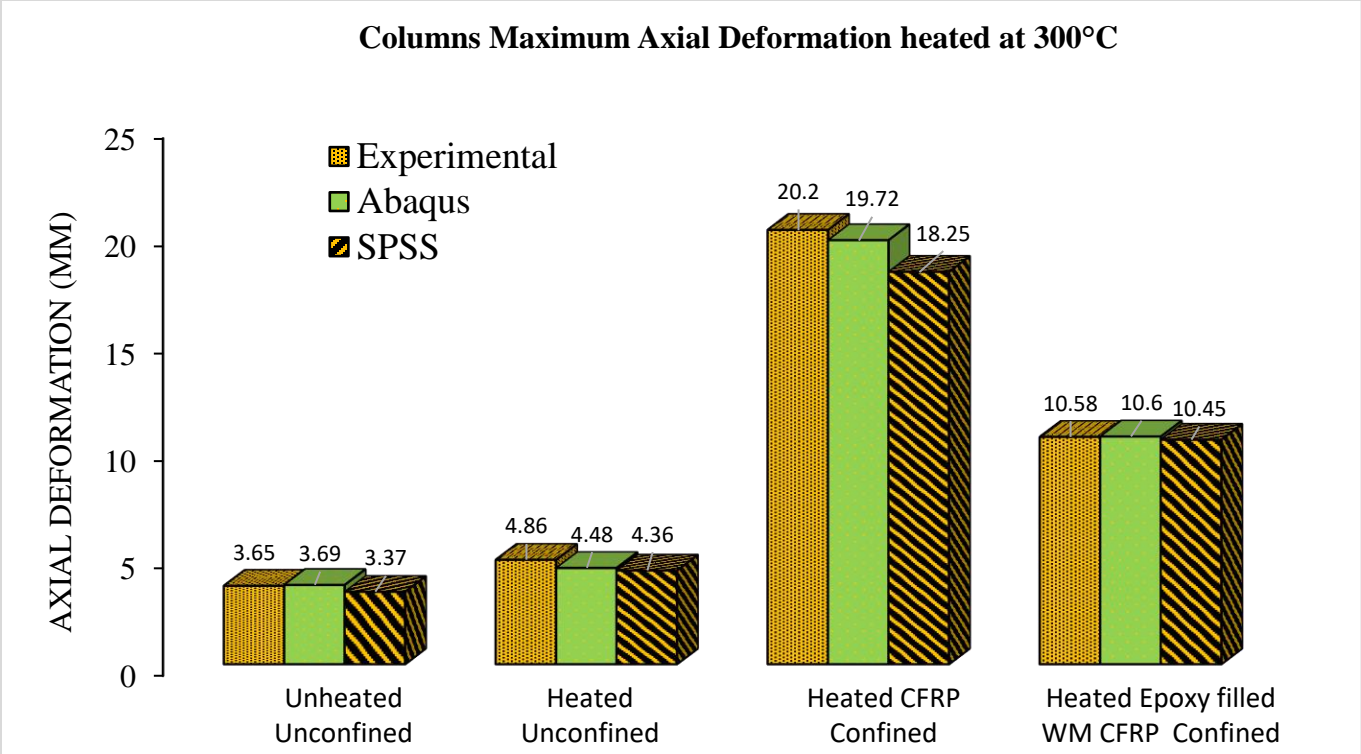
Figure 14: Load vs axial deformation for post-heated (500°C) unconfined column
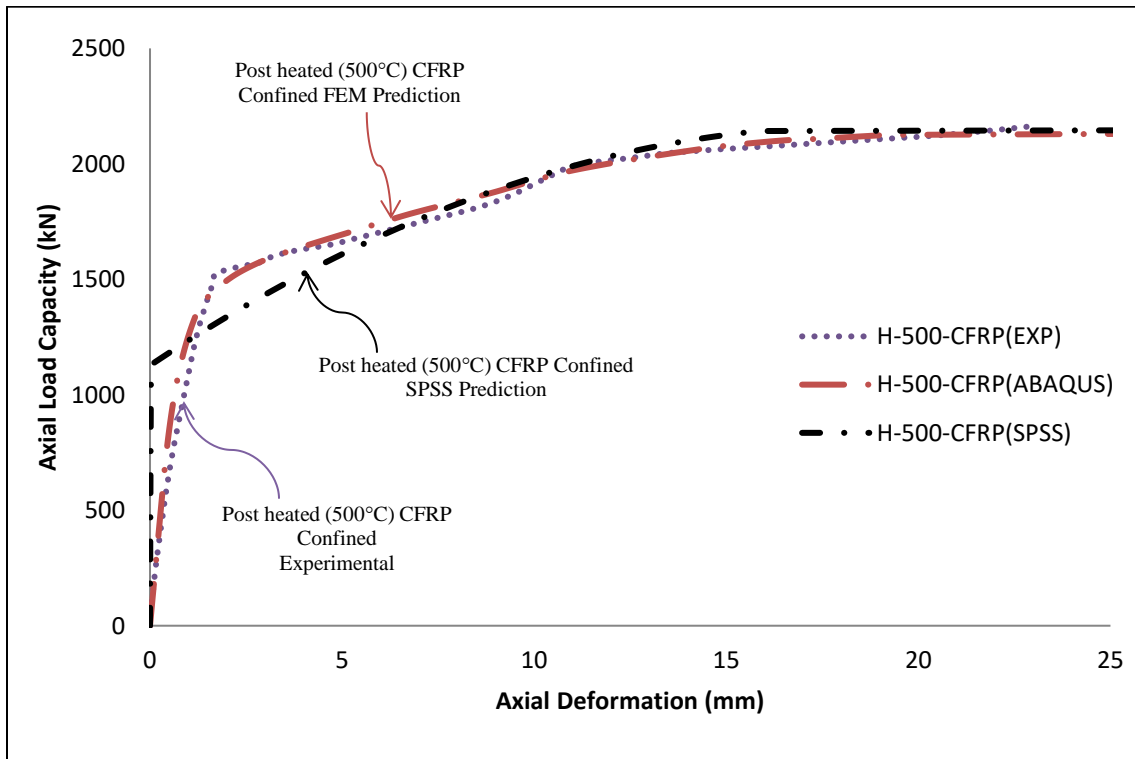
Figure 15: Load vs axial deformation for post-heated (500°C) CFRP confined column
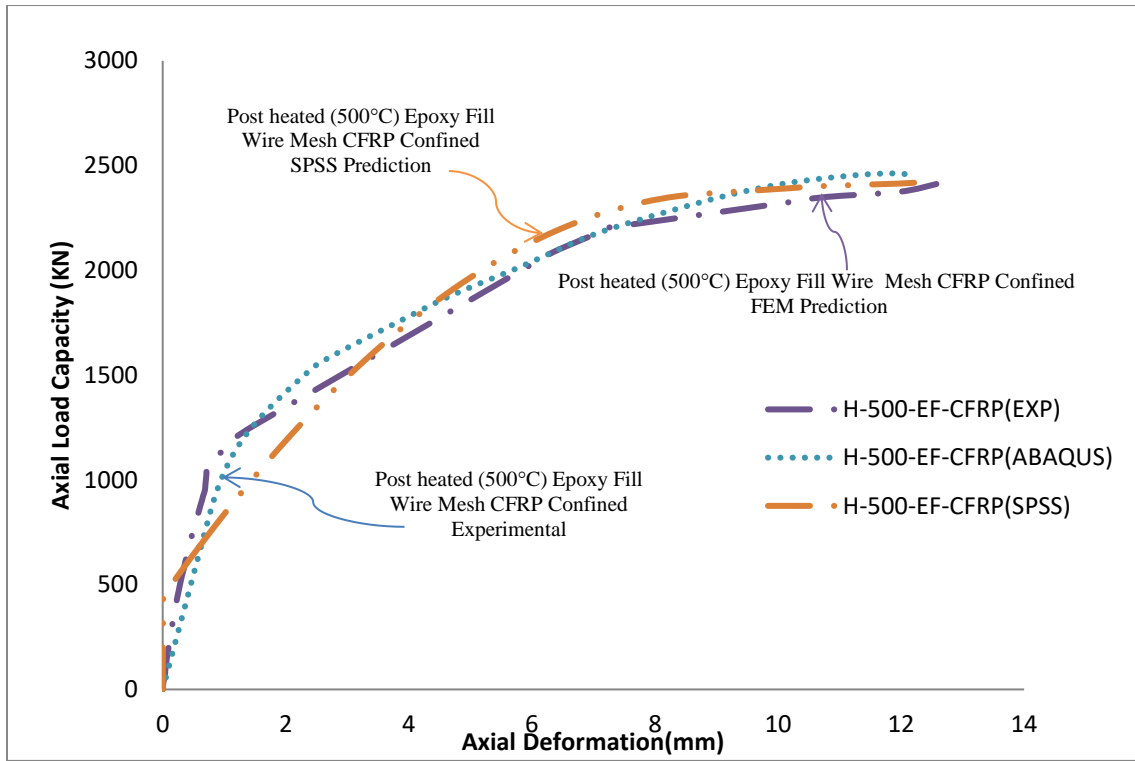
Figure 16: Load vs axial deformation for post-heated (500°C) epoxy fill steel wire mesh covered CFRP confined column
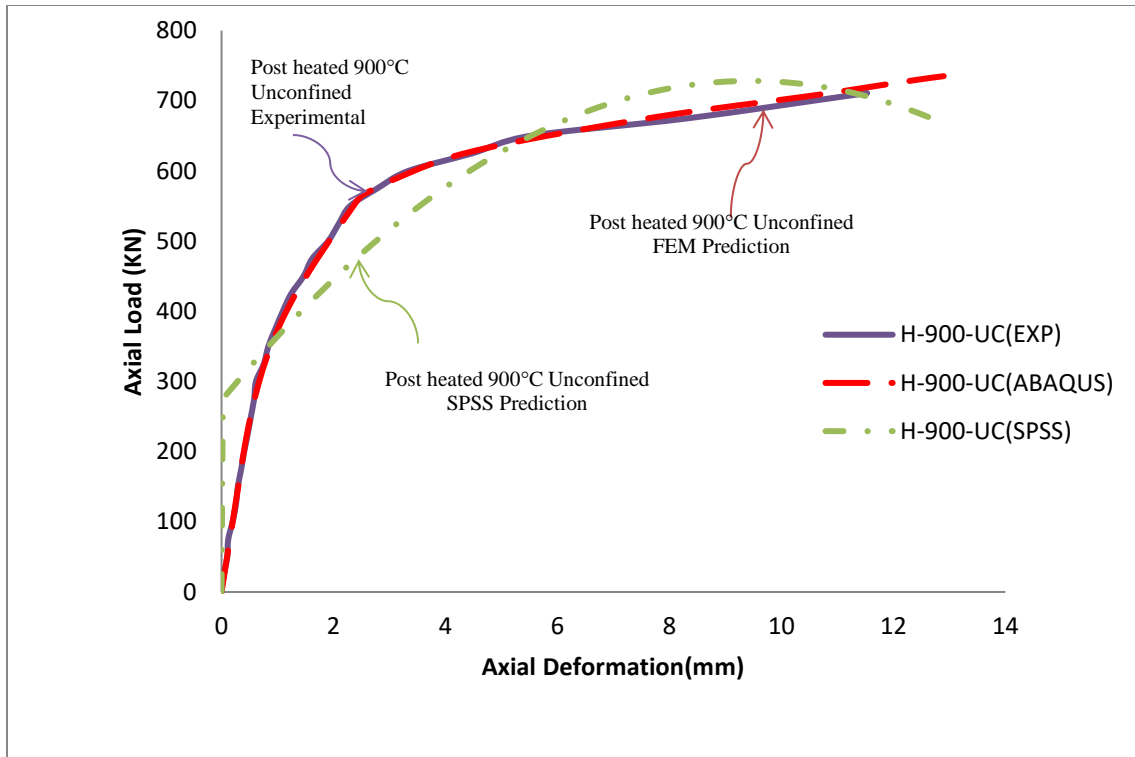
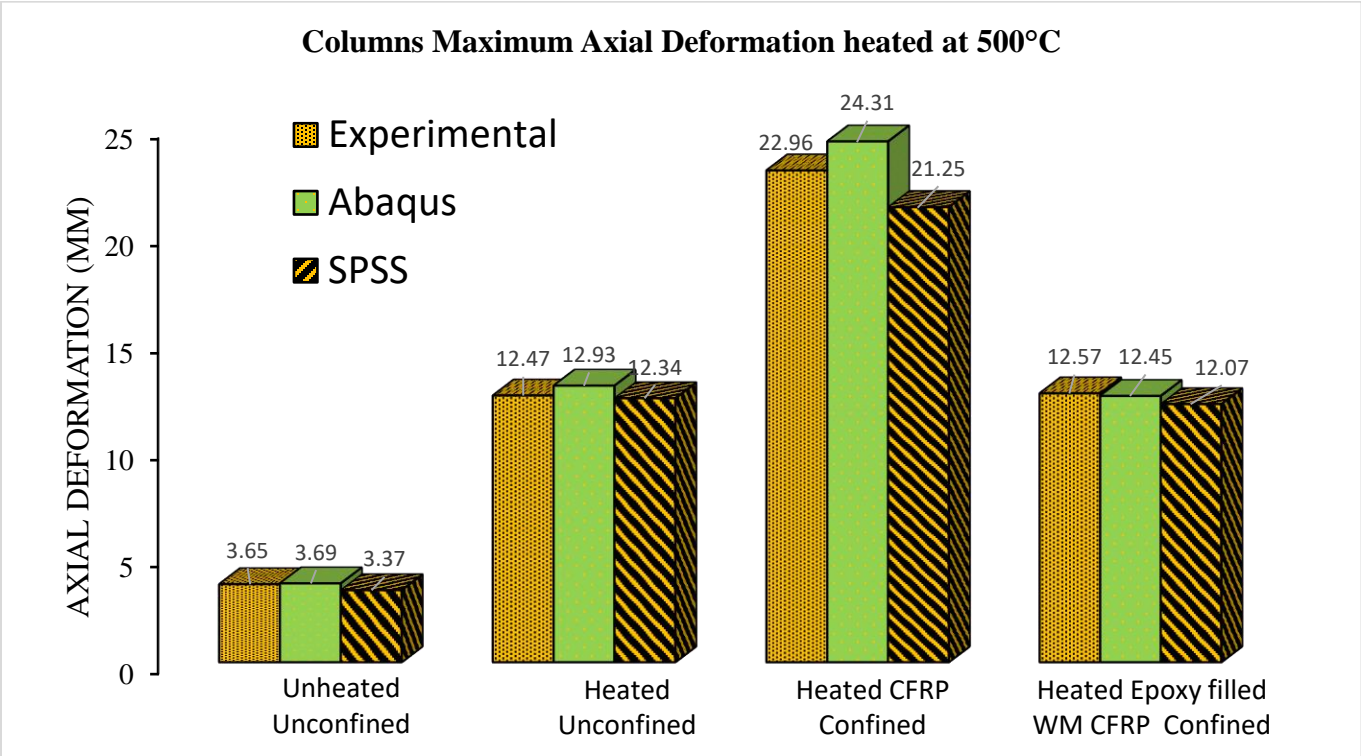Figure 17: Load vs axial deformation for post-heated (500°C) unconfined column

Figure 18: Load vs axial deformation for post-heated (900°C) CFRP confined column

34

Figure 19: Load vs axial deformation for post-heated (900°C) epoxy fill steel wire mesh covered CFRP confined column

Figure 20: Maximum axial deformation comparison for post-heated 300°C columns

Figure 21: Maximum axial deformation comparison for post-heated 500°C columns
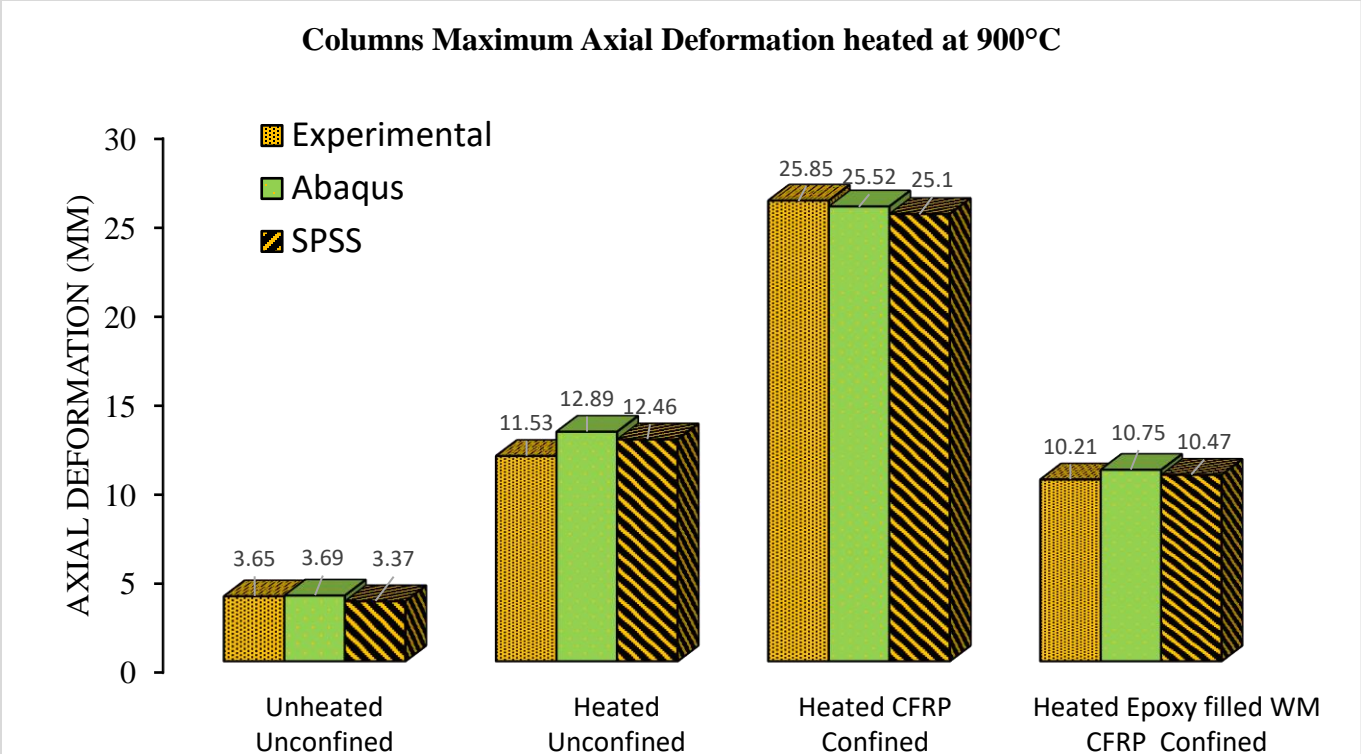
Figure 22: Maximum axial deformation comparison for post-heated 900°C columns

Tables

Table 1: Properties of polypropylene (Sika Fiber 12)

Property	Value	Standard
Density (kg/litre)	0.91	US CONEG Legislation Limit for Heavy Metals, European Directive 94/62/EC of 20.12.94
Fiber length (mm)	12	
Fiber diameter (micron)	18	
Absorption	Nil	
Softening point (°C)	160	
Specific surface area (m^2/kg)	200	
Thermal conductivity	Low	
Alkali resistance (%)	100	
Electrical conductivity	Low	

Table 2: Dry carbon fiber reinforced polymer properties (CFRP Wrap CFW-600)

Property	Value	Standard
Area weight (g/mm^2) Fibers only	610 ± 20	-
Thickness of Fiber (mm)	0.337	-
Density of Fiber (g/cm^3)	1.79	-
Modulus (Tensile) N/mm^2	230,000	ISO 10618
Tensile strength MPa	4,900	
Elongation at break	1.50 %	

Table 3: Properties of CFRP Wrap CFW-600

Property	Value	Standard
7 days tensile strength (N/mm^2) at +23°C	30	DIN 53452
Density (at + 20°C)	1.31 ± 0.1 kg/litre	-
Toxicity	Non-Toxic	DIN 53452
Viscosity	Pasty, does not flow	-
Open time (23°C and 35°C)	30 minutes	-
Pot life (600 ml) 15°C 35°C	90 minutes 30 minutes	-

Table 4: Properties of Sikadur 31 CF Slow

Property	Value
Compressive Strength (MPa) at 7 days and +25°C	48–58
Flexural Strength (MPa) at 7 days and +25°C	23–33
Tensile Strength (MPa) at 7 days and +25°C	11–16
7 days Bond Strength (N/mm2) with Steel at +25°C	13–17
8 days Bond Strength (N/mm2) with Concrete at +25°C	>4
Density (When Evacuated) at +23°C	1.93 kg/litre

Table 5: CFRP Wrap CFW-600 and Chemdur 300 Laminate Properties

Property	Value
Wire thickness (mm)	1.4
Mesh opening	19 mm x 19 mm
Yield strength of wire in tension (N/mm^2)	20.30
Ultimate strength of wire in tension (N/mm^2)	32.48

Table 6: Grouping of columns based on type of tests and repair technique used

Type of Sample	Repair Technique	No. of Samples
Unheated	-	3
Heat damaged at 300°C	Unconfined	2
	CFRP confined	2
	Epoxy fill wire mesh covered CFRP confined	2
Heat damaged at 600°C	Unconfined	2
	CFRP confined	2
	Epoxy fill wire mesh covered CFRP confined	2
Heat damaged at 900°C	Unconfined	2
	CFRP confined	2
	Epoxy fill wire mesh covered CFRP confined	2
Total Samples		21

Table 7: Different parameters of concrete that were finalized after calibration of the model

Parameters	Values
Poisson's ratio, ν	0.14
Angle of dilation	33
Cover (Concrete), mm	30
Size of loading in increments (Max)	0.01
Size of increment (Min)	10–10
E_{cc}	0.1
f_{bo}/f_{c0}	1.16
K	0.67
Viscosity parameter	$1*10^{-5}$

Table 8: Properties of reinforcing bars

Reinforcement type	Mass density	Young's Modulus	Poisson's ratio	Yield Stress	Plastic Strain
Longitudinal and Transverse	7.85E^{-009}	200000	0.3	420	0
Steel Plate	7.85E^{-009}	210000	0.2	---	---

Table 9: General properties of post-heated unconfined concrete

S. No.	Temperature	Fc′ (MPa)	Density (Tons/mm^3)	Elasticity (MPa)
1	300°C	33	2.392×10^{-9}	27000
2	500°C	25	2.387×10^{-9}	23500
3	900°C	18	2.382×10^{-9}	19940

Table 10: General properties of post-heated CFRP confined concrete

S. No.	Temperature	Fc′ (MPa)	Density (Tons/mm^3)	Elasticity (MPa)
1	300°C	67	2.392x10-9	38411
2	500°C	52	2.387x10-9	33892
3	900°C	42	2.382x10-9	30460

Table 11: General properties post-heated epoxy injected steel wire mesh covered CFRP confined concrete

S. No.	Temperature	Fc′ (MPa)	Density (Tons/mm^3)	Elasticity (MPa)
1	300°C	72	2.421×10^{-9}	39880
2	500°C	60	2.417×10^{-9}	36406
3	900°C	56	2.406×10^{-9}	35171

Table 12: Comparison of experimental, regression and finite element models for axial capacity (kN) at 300°C

Description	Exp	FEM	SPSS	% diff. FEM with EXP	% diff. SPSS with EXP
Unheated unconfined	1353	1365	1320	-0.88	2.43
Post-heated 300°C unconfined	1197	1206	1194	-0.746	0.25
Post-heated 300°C CFRP confined	2433	2471	2419	-1.56	0.57
Post-heated 300°C epoxy fill wire mesh covered CFRP confined	2800	2789	2757	0.39	1.53

Table 13: Comparison of experimental, regression and finite element models for axial capacity (kN) at 500°C

Description	Exp	FEM	SPSS	% diff. FEM with EXP	% diff. SPSS with EXP
Unheated unconfined	1353	1365	1320	-0.88	2.43
Post-heated 500°C unconfined	975	1055	941	-8.2	3.48
Post-heated 500°C CFRP confined	2163	2130	2145	1.52	0.83
Post-heated 500°C epoxy fill wire mesh covered CFRP confined	2412	2460	2452	1.95	1.65

Table 14: Comparison of axial load capacity of experimental, regression and finite element models (kN) at 900°C

Description	Exp	FEM	SPSS	% diff. FEM with EXP	% diff. SPSS with EXP
Unheated unconfined	1353	1365	1320	-0.88	2.43
Post-heated 900°C unconfined	711	731	781	-2.81	-9.84
Post-heated 900°C CFRP confined	1763	1688	1738	4.25	-3.42
Post-heated 900°C epoxy fill wire mesh covered CFRP confined	2014	2083	1996	1.41	0.89

Table 15: Comparison of experimental, regression and finite element models of maximum axial deformation in mm at 300°C

Description	Exp	FEM	SPSS	% diff. FEM with EXP	% diff. SPSS with EXP
Unheated unconfined	3.65	3.69	3.37	-1.09	7.67
Post-heated 300°C unconfined	4.86	4.48	4.36	7.81	10.2
Post-heated 300°C CFRP confined	20.20	19.72	18.25	2.37	9.65
Post-heated 300°C epoxy fill wire mesh covered CFRP confined	10.58	10.6	10.45	-0.3	1.97

Table 16: Comparison of experimental, regression and finite element models of maximum axial deformation in mm at 500°C

Description	Exp	FEM	SPSS	% diff. FEM with EXP	% diff. SPSS with EXP
Unheated unconfined	3.65	3.69	3.37	-1.09	7.67
Post-heated 500°C unconfined	12.47	12.93	12.34	-3.68	1.053
Post-heated 500°C CFRP confined	22.96	24.31	21.25	-5.61	8.04
Post-heated 500°C epoxy fill wire mesh covered CFRP confined	12.57	12.45	12.07	0.96	3.97

Table 17: Comparison of experimental, regression and finite element models of maximum axial deformation in mm at 900°C

Description	Exp	FEM	SPSS	% diff FEM with EXP	% diff SPSS with EXP
Unheated unconfined	3.65	3.69	3.37	-1.09	7.67
Post-heated 900°C unconfined	11.53	12.89	12.46	-11.79	-8.06
Post-heated 900°C CFRP confined	25.85	25.52	25.1	1.27	2.86
Post-heated 900°C epoxy fill wire mesh covered CFRP confined	10.21	10.75	10.47	-5.28	-2.54

Table 18: Equations for prediction of axial deformations

Description	Equations Developed
Post-heated unconfined samples	$P_{nuc\theta} = \begin{cases} -23.83\, Þ^2 + 312.43\, Þ + 322 & (100C^0 < \theta \le 300C^0) \\ -5.03\, Þ^2 + 103\, Þ + 385 & (300C^0 < \theta \le 500C^0) \\ -5.10 Þ^2 + 96.38\, Þ + 274.45 & (500C^0 < \theta \le 900C^0) \end{cases}$ $P_{nuc\theta}$ is axial load capacity (kN) and Þ is axial deformation (mm)
Post-heated CFRP confined samples	$P_{ncc} = \begin{cases} -4.64\, Þ^2 + 171.2\, Þ + 877 & (100C^0 < \theta \le 300C^0) \\ -1.86\, Þ^2 + 94.02\, Þ + 1167 & (300C^0 < \theta \le 500C^0) \\ -2.12\, Þ^2 + 84.72\, Þ + 842 & (500C^0 < \theta \le 900C^0) \end{cases}$ P_{ncc} is axial load capacity (kN) and Þ is axial deformation (mm)
Post-heated epoxy injected steel wire mesh, cement sand mortar covered wrapped with CFRP	$P_{nec\theta} = \begin{cases} -76.03\, Þ^2 + 881.79\, Þ + 98.57 & (100C^0 < \theta \le 300C^0) \\ -22.63\, Þ^2 + 418.17\, Þ + 441.3 & (300C^0 < \theta \le 500C^0) \\ -20.52\, Þ^2 + 364.52\, Þ + 389.8 & (500C^0 < \theta \le 900C^0) \end{cases}$ $P_{nec\theta}$ is axial load capacity (kN) and Þ is axial deformation (mm)